Tom Schwartz
- visited - July 25/01

884280
82FSE 014
028

The Iron Range Project

Nelson Mining Division, Southeastern B.C.
Mapsheets 82JF028, 82F029, 82F018, 82F019
Latitude 49°12' N, Longitude 116°24'W

Executive Summary

C.C. Downie, P.Geo
Exploration Manager
Eagle Plains Resources Ltd.
2720-17th Street South
Cranbrook, B.C.
V1C 6Y6

March 3, 2001

Summary

The Iron Range Property consists of 74 2-post claim units located in the Goat River area 15km NE of Creston, BC. The claims are owned 100% by Eagle Plains Resources Ltd., and carry no underlying royalties or encumbrances.

The Iron Range deposits were originally staked in 1897 and were covered by Crown Grants held by Cominco Ltd. and the CPR. When the grants were reverted in 1999, Eagle Plains Resources Ltd. recognized the opportunity to secure the Iron Range deposits and the original 32 FeO and I.R. claims were acquired. Past work on the Iron Range deposit by Cominco Ltd. focused on the considerable iron oxide resource and consisted of trenching and very shallow(20m depth) diamond drilling in the area along the Iron Range Mountain ridge.

Mineralization on the Iron Range Property varies from massive lenses of hematite and magnetite to hematite - magnetite breccia bodies. Mineralization occurs within the Iron Range fault zone, a regional scale, Proterozoic structure. The mineralized zone is exposed over approximately 4 kilometers strike length and is up to 150 meters wide. Structural, mineralization and alteration relationships indicate that the property has potential for both Olympic Dam type Cu – Au - U - REE deposits and Sullivan type sedimentary - exhalitive deposits.

Eagle Plains is seeking to attract participation by a major mining company, and is prepared to relinquish a 60% interest in the property for a modest cash consideration coupled with comprehensive exploration work, according to a mutually agreeable schedule.

Location, Access and Infrastructure

The Iron Range Property is located 15 km northeast of Creston, B.C. near the Goat River, and is accessed by a network of seasonally maintained BC Forest Service roads (Figure 1, following). Elevations range from 1650 - 1900m, with a summer field season ranging from May to mid-November. A well developed transportation and power corridor lies approximately 8 km from the property. A new high pressure gas pipeline and a high voltage hydro-electric line follow the CPR mainline and Highway 3 south of the property boundary. The rail line provides efficient access to the Cominco Ltd. smelter in Trail, B.C.

Tenure

The property consists of 74 2-Post claim units. The FeO 1 – 30 and the IR 1 – 36 are located north of the highway in the area of the main Iron Range deposits. The TCK 1-8 are located south of the highway in the Thompson Mountain area. The claims are owned 100% by Eagle Plains Resources Ltd. A claim location map

Eagle Plains Resources - IRON RANGE PROJECT

BC Administrative Area Layers

BC Communities
- City
- Town
- Village
- Resort Municipality
- Settlement
- Community
- District Municipality

Parks Layers

Parks - Proposed SEBC

Mineral Titles Layers

Mineral titles outline (<1M)
All Others

Topographic Layers

Railways 1:6M

Roads 1:250K (<2M)

Rivers 1:250K (<2M)

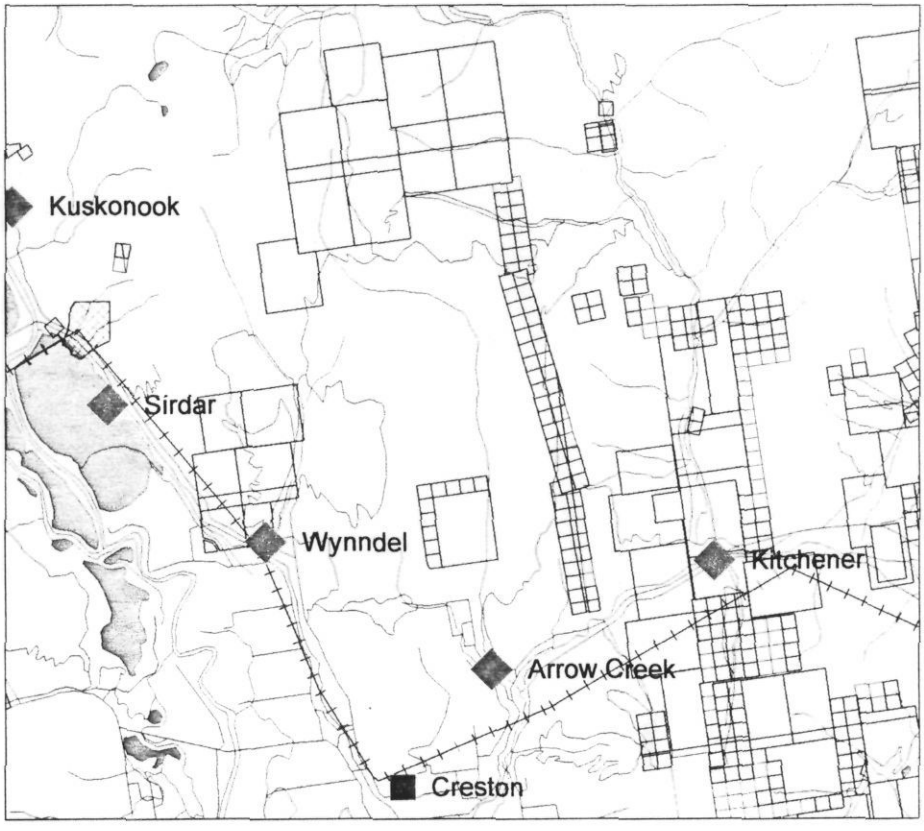

SCALE 1 : 267,488

2 0 2 4 6

MILES

N

http://ebony.gov.bc.ca/mapplace/maps/minpot/dep_find.MWF

Wednesday, March 07, 2001 1:27 PM

map and list of all pertinent tenure details is provided in Appendix I, following this report.

History and Previous Work

The Iron Range prospect was discovered and staked in 1897 along an extensive belt of iron oxide showings. Initial work included several small shafts, adits, and trenches, as well as limited diamond drilling to a maximum depth of 20 meters. Many of the original claims on the Iron Range were established as Crown Grants. In 1939, The Consolidated Mining and Smelting Company of Canada Ltd., along with its parent company Canadian Pacific Railroad(CPR), acquired the main claim block on the northern part of Iron Range Mountain. The claims were evaluated by CM&S, now called Cominco Ltd., to assess the potential for a large iron resource. As part of this evaluation, Cominco completed an extensive trenching program in 1957, exposing the Iron Range structure and mineralization over more than 4 kilometers strike length. Most of the Iron Range Crown Grants were held by Cominco – CPR until 1999, when they were reverted. Eagle Plains Resources Limited restaked the original Crown Grants as the FeO and I.R. claims on the day the historic grants lapsed.

Geology

Regional Geology

The Iron Range occurrence is underlain by the peri-cratonic Proterozoic Purcell SuperGroup, a 5000m thick succession of siliclastic and lesser carbonate rocks. Iron Range Mountain is underlain by sediments of the Middle Aldridge Formation and several concordant Moyie sills. These rocks form the core of the Goat River anticline, a broad, gently plunging fold which underlies the west half of the Yahk map area(Brown and Stinson, 1995). The Iron Range Fault is a steeply dipping, north striking structure which cuts the core of the Goat River anticline. The fault cuts upsection south from the International Boundary, in Lower Aldridge Formation, to Upper Aldridge Formation just north of the Yahk map area. Mineralization and deformation zones associated with this structure vary from 10 meters width near the 49th parallel to 150 meters width on the northern part of Iron Range Mountain. The fault is characterized by strong alteration along its entire length, as well as local high concentrations of iron oxide mineralization.

The scale of the deformation, and the complex relationships between deformation and mineralization, point to a protracted, possibly multi-stage history for the Iron Range occurrences (Brown and Stinson, 1995). Rare kinematic indicators associated with the mineralized fault, local drag folding and offsets in Aldridge Formation marker horizons provide evidence for both west -side down movement and possibly bi-directional strike-slip movement. (D. Anderson,

Cominco Ltd.; in Brown and Stinson, 1995). Deformation in the surrounding rocks consists of penetrative cleavage and local meter scale folding. North-northwest plunging fold axes and intersection lineations are best developed near the fault and are genetically related to it.

Iron Range Mineralization(Fig.2)

Mineralization and alteration associated with the Iron Range fault is varied and is generally divided into a number of geographic zones. The Main Zone (FeO 2,4... 14,16 Claims) is located on the widest part of the fault zone. The historic X-Ray Crown Grant in the north and the Rhodesia in the south bound the zone. Lenses of massive hematite and magnetite ranging from 0.5 - 3 meters width occur along approximately 3 km strike length in dilation zones ranging from 60 meters to 150 meters wide. The zone was the focus of the Cominco Ltd. 1957 trenching program. Brown and Stinson mapped a continuous exposure preserved in trenches on the historic Maple Leaf claims. There the zone was found to consist of four parallel lenses spaced from 5 to 40 meters apart. Iron content within the massive mineralization is reported as high as 55.2% (EMPR Minfile 082FSE018).

These massive lenses are surrounded by wider zones of hematite breccia. The breccia consists of fragments of albitite in a hematite rich matrix. A two to six meter wide microbreccia occurs in contact with the iron lenses. This grades outward into wider cataclastic breccia zones with hematite as both matrix and veins. Mineralogically the lenses and breccias are dominantly hematite with variable amounts of original magnetite ranging from 5 to 30 percent. Sulphide minerals are rare in the Iron Range Main Zone, with the exception of the northernmost Cominco trenches. Here 3-4% pyrite occurs as anhedral blebs in both iron lenses and iron breccias.

Several types of alteration are associated with the Iron Range deposit. The highest grade iron mineralization is typically associated with albite alteration. In the Main Zone, fine grained ,sugary albite extends over most of the width of the fault zone. The albite appears to be contained by the fault zone, and is surrounded by a wide zone of sericitic alteration that extends 500 - 1000 meters from the Iron Range fault.

Sheared gabbro bodies are found along the width of the Main Zone fault. Mineralization associated with these foliated gabbros includes massive hematite lenses, foliation parallel veins and hematite–magnetite disseminations. The background level of magnetite in these sheared gabbros (0.5 – 1% disseminated magnetite) distinguishes it from the typical Moyie sills in the area which are non magnetic and do not register on the regional aeromagnetic map. The gabbro bodies are characterized by strong, parallel to strike foliation and strong chlorite alteration related to the shearing event.

rest of the Iron Range fault and subsiduary faults). The main deposit produces a continuous, prominent aeromagnetic anomaly (Geological Survey of Canada, 1971).

MAIN ZONE

The main Iron Range deposit is contained within the widest segment of the fault zone. The deposit varies in width from approximately 60 to 150 metres and is at least 3 kilometres long. It runs from the Union Jack claim in the north to the Rhodesia claim in the south (MINFILE 082FSE014-20). This is the area explored by Cominco's 1957 trenching program. Bedrock is exposed in the less-deteriorated trenches; natural outcrop is very rare. Deformation fabrics, veining, and mineralized zones are all strongly aligned in the fault zone and are related to movement across it.

Lenses of massive hematite and magnetite occur along the length of the main zone. They range in width from 0.5 to 3 metres and pinch and swell substantially over their strike length. They are difficult to trace from trench to trench. Where nearly continuous exposure across the fault zone is preserved in trenches on the Maple Leaf claim, there are four parallel lenses spaced from 5 to 40 metres apart (Figure 2).

Most of the massive lenses are surrounded by wider zones of hematite breccia. Less commonly, massive iron oxide lenses cut foliated, sericitic sediments or gabbro. Breccia consists of fragments of albitite in a hematite-rich matrix. Contacts between the breccia and the

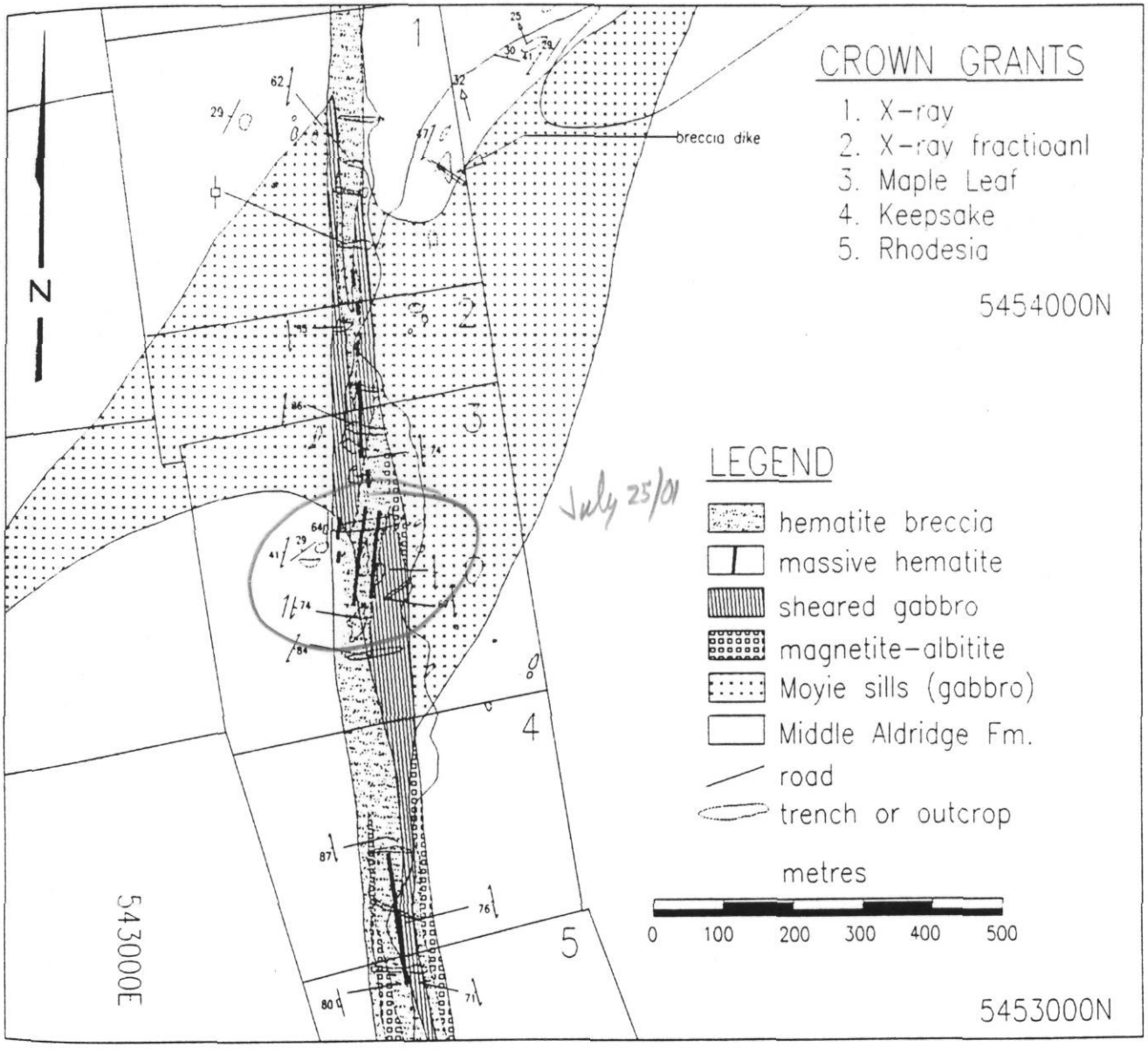

Figure 2. Detailed map of the part of the Iron Range fault and mineralization. See Figure 6 for location.

Other zones along the Iron Range structure include the La Grande, the Mount Thompson and the Crackerjack occurrences. On the La Grande(Fe02 Claim), the fault zone is 20 - 40 meters wide; mineralization occurs as massive lenses of iron oxide associated with grey quartz and hematite alteration. The Mount Thompson occurrence is a 1-2 meter wide albitite zone with disseminated to semi-massive magnetite. The albitite is surrounded by an envelope of hematitic fractures. The vertical zone cuts flat lying sediments, and appears to be part of a wider, anastomosing set of faults. The Mount Thompson is located south of Highway 3 and is covered by the TCK1 – 8 claims. The Crackerjack fault is a parallel trending structure located east of the Main Zone. The poorly exposed structure consists of hematite - albitite breccia, and returned values of up to 34% Fe2O3.

Discussion and Exploration Model

The Iron Range Fault and the Iron Range deposit are evidence of a long lasting, multi - stage structural event. Initial movement on the Iron Range Fault is believed to be associated with growth faults in buried Aldridge Formation sediments. These growth faults may have acted as conduits for feeder dykes to the Moyie sills. Within the Iron Range Fault, these sills became structurally deformed, forming the long, narrow gabbro bodies found within the Iron Range structure. This initial episode was associated with strong hydrothermal albite alteration along the sill contacts as they intruded relatively unconsolidated, water laden sediments along the shallow sea floor. This albitic alteration is associated with weak magnetite alteration and was followed by the main Iron Range deformation and mineralization event.

In the wide Main Zone, deformation consisted of extensive cataclastic brecciation of albitite, foliation of gabbro sills and local development of slaty cleavage in sericitic sediments. Breccia styles range from cataclasites to protocataclasites, and gabbros within the fault zone are mylonitic. This wide range of deformation types is typical of an episode that occurs at several kilometers depth (Ramsay and Huber, 1987). This main event constituted the ground preparation for the main mineralizing episode. Fine grained hematite formed large, fault parallel lenses and replaced fault gouge in the breccias. Initial magnetite deposition was followed by the more abundant hematite as mineralizing fluids became more oxidized. Further deformation occurred after the main mineralizing episode. Hematite - magnetite rich rocks have been overprinted by fractures, shear veins and ductile folds.

Hydrothermal iron deposits have received attention due to recent findings at the Olympic Dam deposit in Australia. Early interpretations defined the deposit as forming during diagenetic mineralization and alteration of sedimentary breccias. More recent work has established the hydrothermal nature of the breccias and recorded evidence for near surface hydrothermal brecciation within the host granitic batholith. Copper, gold, silver, uranium and rare earth elements were

deposited late in the evolution of the breccias and later enriched by supergene processes. The core zone of the breccia body is associated with a topographic lineament thought to reflect an underlying fault zone.

The Iron Range Fault system represents a major structural feature that is markedly different from other structures in the area in terms of deformation and alteration. The Iron Range deposits are directly linked to this structure which has a strike length of at least 90 kilometers. The world class Sullivan deposit, located approximately 50 km northeast of the Iron Range deposits, formed in a sub-basin near the contact between the Lower and Middle Aldridge Formation. It is believed that deep seated Proterozoic structures also influenced the formation of the Sullivan sedimentary – exhalitive deposit. Probably starting as a growth fault, this older structure acted as a locus for Moyie sill intrusion and arching, as well as a conduit to metal enriched hydrothermal solutions, which were issued from vents formed along the fault trace. At the Sullivan, an initial period of tourmalinization was followed by a series of sulphide mineralizing events. Initially very rapid, the mineralizing event was protracted and followed by at least two pulses of sericite / albitite alteration. The wide range and timing of the mineralization and alteration events at the Sullivan point toward the existence of a deep seated, Proterozoic structure that acted as access to basement derived fluids. RGS geochemical data indicates that many of the streams within the Iron Ridge deposit area have anomalous zinc, lead, gold, copper, antimony and arsenic values. The general pattern of this broad anomaly suggests that the source is likely related to a northwest trending structure.

Conclusions and Recommendations

The Iron Range Fault Structure should be systematically evaluated for Olympic Dam and Sullivan type deposits. Quantitative analyses by the BC Department of Energy, Mines and Petroleum Resources of the geological data for the Iron Range area place it in the category of highest potential for mineral deposits in the province. Initial work should include extending the claim coverage north and south to include areas where the Iron Range structure is buried, and east and west to cover possible lateral mineralization associated with the structure. Ground work should include heavy mineral sampling in the Iron Range Mountain area drainages, as well as regional sampling along the Iron Range Fault. The geomagnetic signature of the gabbro bodies associated with the Iron Range Fault System could be the basis for a useful regional exploration tool and the existing aeromagnetic map should be re examined in this light. The vertical nature and tremendous strike and dip extent of the Iron Range Fault Structure make it a very attractive drill target. In light of the association of the Sullivan deposit with a similar large scale deep seated structure, an obvious target would be to test the Sullivan stratigraphic horizon near the projected intersection of the Iron Range Fault and the Lower - Middle Aldridge formation contact.

Appendix I

Tenure Details

IRON RANGE PROPERTY

Claim Name	Record No.	Claim Type	No. of Units	Map Number	Expiry Date
FeO 1	379349	2P	1	082F028	July 25, 2001
FeO 2	379350	2P	1	082F028	July 25, 2001
FeO 3	379351	2P	1	082F028	July 25, 2001
FeO 4	379352	2P	1	082F028	July 25, 2001
FeO 5	379353	2P	1	082F028	July 25, 2001
FeO 6	379354	2P	1	082F028	July 25, 2001
FeO 7	379355	2P	1	082F028	July 25, 2001
FeO 8	379356	2P	1	082F028	July 25, 2001
FeO 9	379357	2P	1	082F028	July 25, 2001
FeO 10	379358	2P	1	082F028	July 25, 2001
FeO 11	379359	2P	1	082F028	July 25, 2001
FeO 12	379360	2P	1	082F028	July 25, 2001
FeO 13	379361	2P	1	082F028	July 25, 2001
FeO 14	379362	2P	1	082F028	July 25, 2001
FeO 15	379363	2P	1	082F028	July 25, 2001
FeO 16	379364	2P	1	082F028	July 25, 2001
FeO 17	381631	2P	1	082F028	October 21, 2001
FeO 18	381632	2P	1	082F028	October 21, 2001
FeO 19	381633	2P	1	082F028	October 21, 2001
FeO 20	381634	2P	1	082F028	October 21, 2001
FeO 21	381635	2P	1	082F028	October 21, 2001
FeO 22	381636	2P	1	082F028	October 21, 2001
FeO 23	381637	2P	1	082F028	October 21, 2001
FeO 24	381638	2P	1	082F028	October 21, 2001
FeO 25	381639	2P	1	082F028	October 21, 2001
FeO 26	381640	2P	1	082F028	October 21, 2001
FeO 27	381641	2P	1	082F028	October 21, 2001
FeO 28	381642	2P	1	082F028	October 21, 2001
FeO 29	381643	2P	1	082F028	October 21, 2001
FeO 30	381644	2P	1	082F028	October 21, 2001
IR 1	379365	2P	1	082F028	July 25, 2001
IR 2	379366	2P	1	082F028	July 25, 2001
IR 3	379367	2P	1	082F028	July 25, 2001
IR 4	379368	2P	1	082F028	July 25, 2001
IR 5	379369	2P	1	082F028	July 25, 2001
IR 6	379370	2P	1	082F028	July 25, 2001
IR 7	379371	2P	1	082F028	July 25, 2001
IR 8	379372	2P	1	082F028	July 25, 2001
IR 9	379373	2P	1	082F028	July 25, 2001
IR 10	379374	2P	1	082F028	July 25, 2001
IR 11	379375	2P	1	082F018	July 25, 2001
IR 12	379376	2P	1	082F018	July 25, 2001
IR 13	379377	2P	1	082F018	July 25, 2001
IR 14	379378	2P	1	082F018	July 25, 2001
IR 15	379379	2P	1	082F019	July 25, 2001
IR 16	379380	2P	1	082F019	July 25, 2001
IR 17	381681	2P	1	082F018	October 24, 2001
IR 18	381682	2P	1	082F018	October 24, 2001
IR 19	381683	2P	1	082F018	October 24, 2001
IR 20	381684	2P	1	082F018	October 24, 2001
IR 21	381685	2P	1	082F018	October 24, 2001
IR 22	381686	2P	1	082F018	October 24, 2001
IR 23	381687	2P	1	082F018	October 24, 2001
IR 24	381688	2P	1	082F018	October 24, 2001
IR 25	381689	2P	1	082F018	October 24, 2001
IR 26	381690	2P	1	082F018	October 24, 2001
IR 27	381691	2P	1	082F018	October 24, 2001
IR 28	381692	2P	1	082F018	October 24, 2001
IR 29	381693	2P	1	082F018	October 24, 2001
IR 30	381694	2P	1	082F018	October 24, 2001
IR 31	381695	2P	1	082F018	October 24, 2001
IR 32	381696	2P	1	082F018	October 24, 2001
IR 33	381697	2P	1	082F018	October 24, 2001
IR 34	381698	2P	1	082F018	October 24, 2001
IR 35	381699	2P	1	082F018	October 24, 2001
IR 36	381700	2P	1	082F018	October 24, 2001
TCK 1	382479	2P	1	082F018	November 16, 2001
TCK 2	382480	2P	1	082F018	November 16, 2001
TCK 3	382481	2P	1	082F018	November 16, 2001
TCK 4	382482	2P	1	082F018	November 16, 2001
TCK 5	382483	2P	1	082F018	November 16, 2001
TCK 6	382484	2P	1	082F018	November 16, 2001
TCK 7	382485	2P	1	082F018	November 16, 2001
TCK 8	382486	2P	1	082F018	November 16, 2001
		TOTAL:	74	units	

References

Geological Survey of Canada (1971): Aeromagnetic Map 8471G, Yahk, British Columbia

C. Lowe, D.A. Brown, M.E. Best, and R.B.K. Shives (2000) : High Resolution Geophysical Survey of the Purcell Basin and Sullivan Deposit: Implications for Bedrock Geology and Mineral Exploration

Hoy, T. (1993) Geology of the Purcell SuperGroup in the Fernie West-half map area, Southeastern British Columbia; BCEMPR Bulletin 84

Hoy T. and Carter, G. (1988): Geology of the Fernie West ½ Map Sheet (and Part of Nelson East ½). British Columbia Ministry of Energy, Mines and Petroleum Resources; Open File Map No. 1988-14.

Stinson, P. and Brown, D. (1994): Iron Range Deposits, Southeastern British Columbia (82F1) Geological Survey of Canada, Geological Fieldwork 1994, paper 1995-1

BCEMPR The MapPlace

BCEMPR MINFILE 082FSE015, 082FSE016, 082FSE017, 082FSE018, 082FSE020, 082FSE021 082FSE023, 082FSE024, 082FSE025, 082FSE026

Appendix II

Iron Range Deposits, SE BC

IRON RANGE DEPOSITS, SOUTHEASTERN BRITISH COLUMBIA (82F/1)

By P. Stinson and D.A. Brown

(Contribution No. 27, Sullivan-Aldridge Project)

KEYWORDS: Economic geology, Proterozoic, Iron Range, albite alteration, breccias, hydrothermal iron oxide deposits.

INTRODUCTION

The Iron Range fault is a steeply dipping north-striking structure in the core of the Goat River anticline, east of Creston. It is characterized by strong alteration along its entire length, and locally, by high concentrations of iron oxide mineralization. Similar alteration was observed along minor subsidiary faults in the northwest and northeast parts of Iron Range Mountain. The main Iron Range deposit consists of the segment of the fault containing the richest iron mineralization and underlies the northern half of the ridge which makes up Iron Range Mountain. This area extends northward onto the Grassy Mountain sheet (82F/8).

The area of most substantial mineralization, where the fault zone runs along the northern part of the crest of Iron Range Mountain, was the focus of a detailed study involving 1:5000 mapping, sample collection, and thin section study of representative samples. The remainder of the Iron Range fault and subsidiary faults with similar alteration were examined and sampled during the course of regional mapping in the Yahk map area (Brown and Stinson, 1995, this volume).

REGIONAL GEOLOGY

Iron Range Mountain is underlain by sediments of the middle Aldridge Formation and several concordant Moyie sills which dip gently to the north and northwest (Figure 1). These rocks comprise the core of the Goat River anticline, a broad, gently north-plunging fold which underlies the west half of the Yahk map area (Brown and Stinson, 1995, this volume). The Iron Range fault is a northerly trending structure which cuts up-section from the International Boundary, in lower Aldridge Formation, to upper Aldridge Formation just north of the Yahk map area; further north it is cut by the Arrow thrust system (Reesor, 1981; Figure 1). It consists of a steeply dipping zone of deformation and mineralization varying in width from about 10 metres near the 49th Parallel to about 150 metres on the northern part of Iron Range Mountain. Net slip on the fault is minor in the main deposit area as sills are offset very little.

However, the amount of deformation and the complex relationships between deformation and mineralization point to a protracted, perhaps multistage history. There is evidence for both west-side-down movement and possibly both directions of strike-slip movement, based on rare kinematic indicators in the mineralized fault, local drag folding, and offsets of marker laminites (D. Anderson, Cominco Ltd., personal communication, 1994). Deformation in the surrounding rocks consists of penetrative cleavage, mainly in silty beds, and local metre-scale folding. Intersection lineations and fold axes in the rocks near the fault have a consistent moderate plunge to the north-northwest. This deformation is strongest near the fault and is probably related to it.

EXPLORATION HISTORY

The Iron Range prospect was discovered and staked in 1897. Over the next five years several shafts, adits, drill holes, and trenches were completed (Blakemore, 1902; Langley, 1922; Young and Uglow, 1926), none of which are preserved. Shafts and drill holes attained a maximum depth of 20 metres below the surface. Cominco Ltd. (then a subsiduary of Canadian Pacific Railways) acquired the main claim block on the northern part of Iron Range Mountain in 1939 and completed a major surface trenching program in 1957. All the exploration activity up to this point was aimed at evaluating the iron resource, which is potentially substantial. The claims remained CPR and Cominco Crown grants until 1994, when they were acquired by Discovery Consultants of Vernon who intend to evaluate the deposit's potential as an Olympic Dam type copper-gold-silver resource.

IRON MINERALIZATION

The intensity and types of mineralization and alteration vary over the length of the Iron Range fault. Mineralized zones can be broadly subdivided into the main deposit (most of the detailed study area), the La Grande zone (the southern part of the detailed study area, named after one of the claims), the Mount Thompson zone (the segment of the fault zone exposed east of the summit of Mount Thompson), and peripheral zones (the

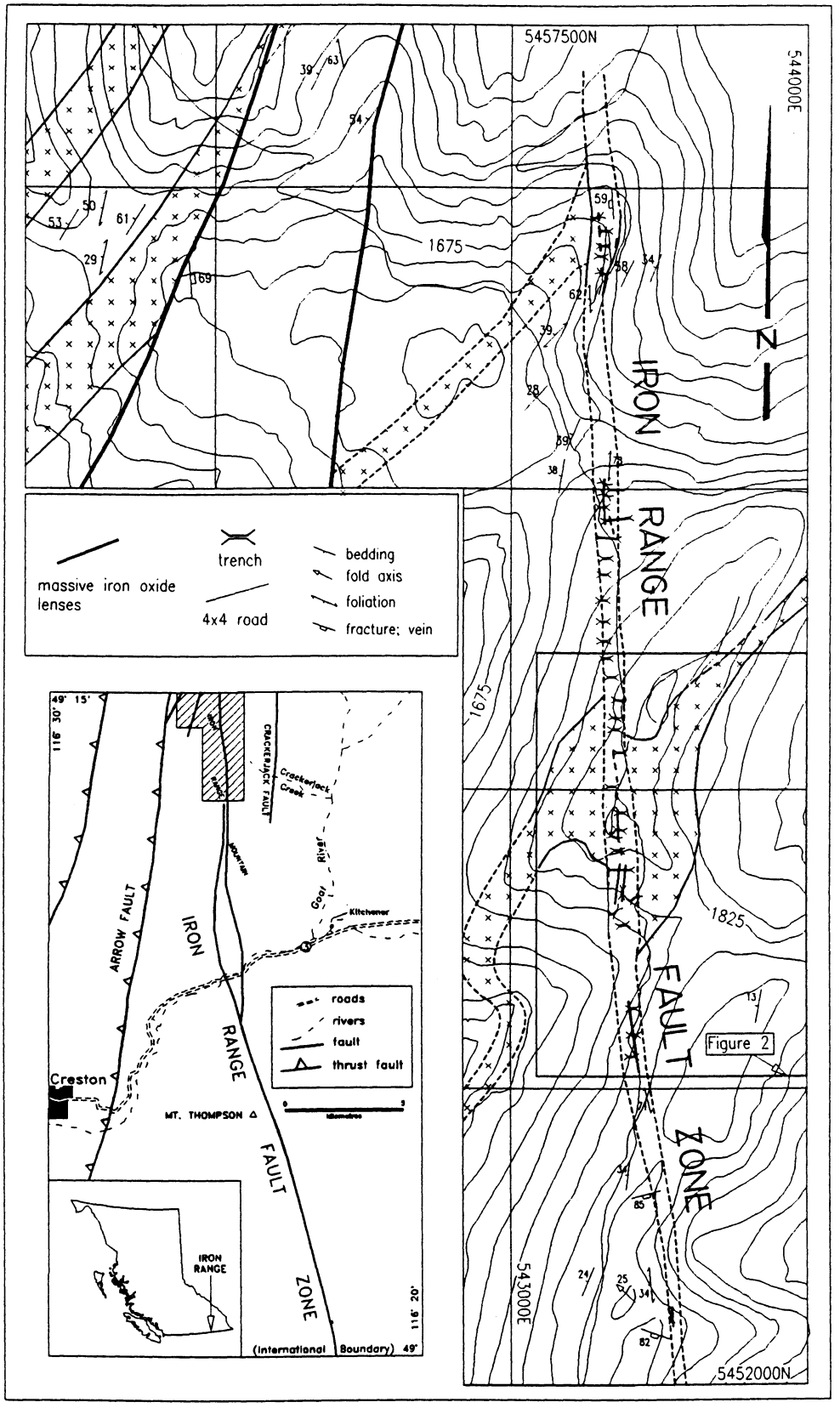

Figure 1. Simplified geological map of the main zone of the Iron Range deposit. Moyie sills are indicated by a cross hatch pattern. The widening of the sills near the fault is mainly a topographic effect. The location of Figure 2 is indicated by the labelled box. The contour interval is 30 metres, and the grid is a 1 kilometre UTM grid. The inset map is the west half of the Yahk map area (simplified from Brown and Stinson, 1995) with the location of the Iron Range map indicated by the hatched area

rest of the Iron Range fault and subsiduary faults). The main deposit produces a continuous, prominent aeromagnetic anomaly (Geological Survey of Canada, 1971).

MAIN ZONE

The main Iron Range deposit is contained within the widest segment of the fault zone. The deposit varies in width from approximately 60 to 150 metres and is at least 3 kilometres long. It runs from the Union Jack claim in the north to the Rhodesia claim in the south (MINFILE 082FSE014-20). This is the area explored by Cominco's 1957 trenching program. Bedrock is exposed in the less-deteriorated trenches; natural outcrop is very rare. Deformation fabrics, veining, and mineralized zones are all strongly aligned in the fault zone and are related to movement across it.

Lenses of massive hematite and magnetite occur along the length of the main zone. They range in width from 0.5 to 3 metres and pinch and swell substantially over their strike length. They are difficult to trace from trench to trench. Where nearly continuous exposure across the fault zone is preserved in trenches on the Maple Leaf claim, there are four parallel lenses spaced from 5 to 40 metres apart (Figure 2).

Most of the massive lenses are surrounded by wider zones of hematite breccia. Less commonly, massive iron oxide lenses cut foliated, sericitic sediments or gabbro. Breccia consists of fragments of albitite in a hematite-rich matrix. Contacts between the breccia and the

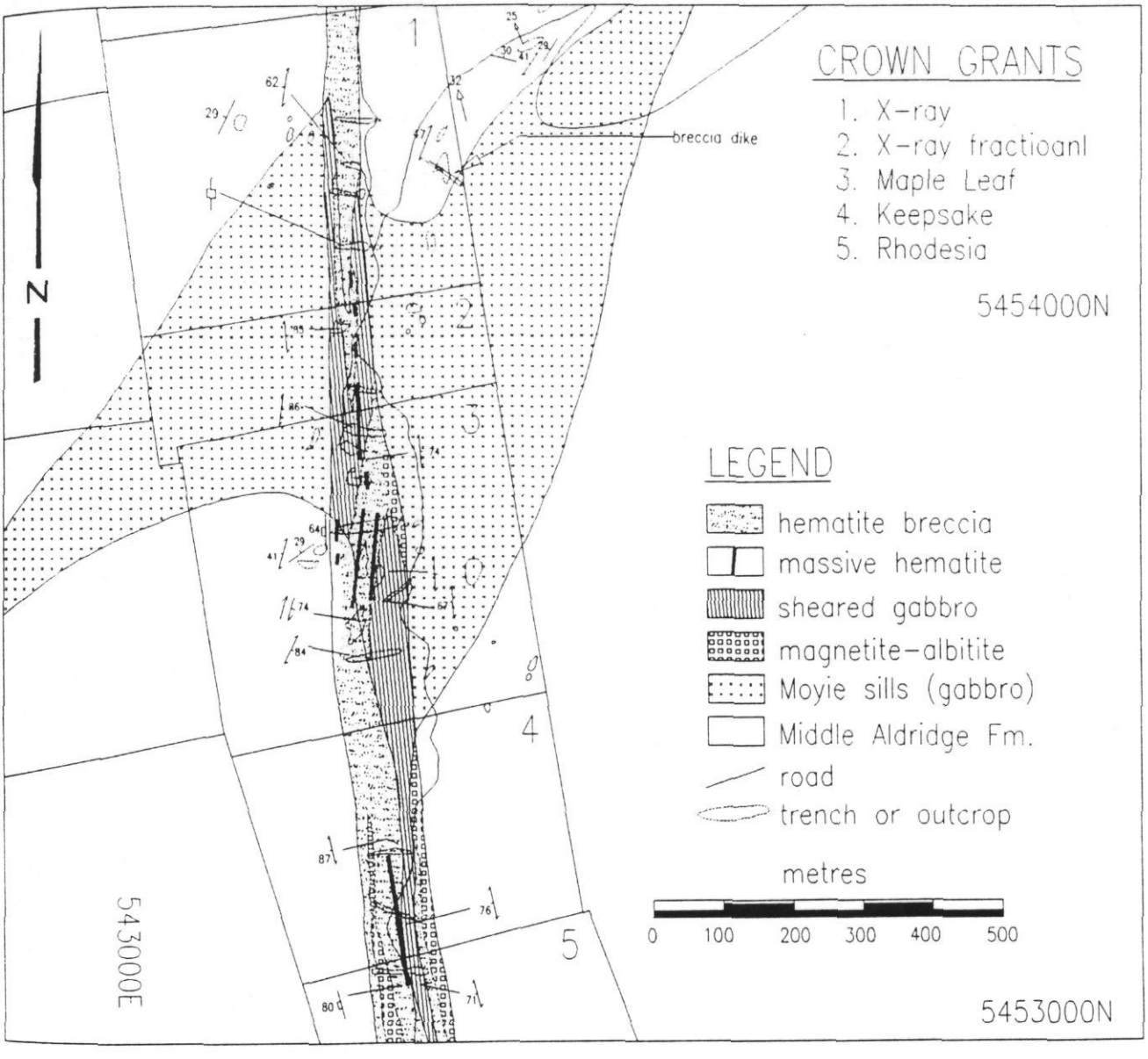

Figure 2. Detailed map of the part of the Iron Range fault and mineralization. See Figure 6 for location.

massive lenses are often gradational as the abundance of clasts diminishes into the lenses. Rare, small, angular fragments of albitite were observed in some of the lenses. Most of the massive lenses have envelopes of microbreccia 2 to 6 metres wide which have 70-80% hematite matrix surrounding angular clasts less than 1 centimetre across. Outward from the hematite-rich zones are wider breccia zones with 30 to 50% hematite as matrix and veins (Photos 1, 2). These breccias have a cataclastic texture. The original matrix is very fine grained fault gouge which is extensively replaced by hematite and minor magnetite. The massive lenses and surrounding breccias constitute the main iron resource of the Iron Range deposit.

The mineralogy of the lenses and breccias is dominantly hematite with variable amounts of magnetite. Thin sections show original magnetite abundances ranging from 5 to 30% as 0.5 to 2-millimetre euhedra. They are strongly pseudomorphed by hematite, with cores of magnetite remaining (Photo 3). The magnetite pseudomorphs sit in a matrix of fine-grained, often radiating, bladed hematite. Parts of the fault zone are occupied by unfractured albitite with disseminated to semimassive magnetite. Large magnetite euhedra (1-5 mm) form local, heavy disseminations, and fine-grained magnetite forms discontinuous veinlets and pods.

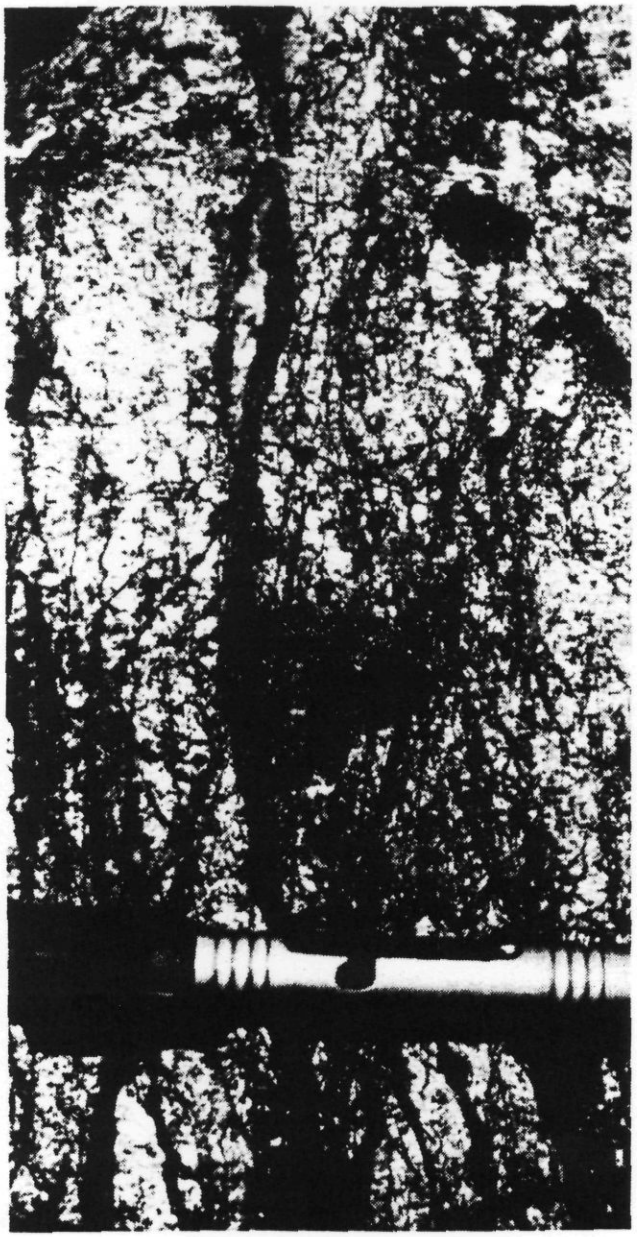

Photo 1. A cataclastic breccia from the main Iron Range deposit. The fracture filling is largely hematite and the rest is albitite (hand sample DBR93-220). The large dark spots are lichen. Flare pen for scale.

Sulphide minerals are rare in the Iron Range fault, with the exception of the northernmost trenches. In these trenches there is up to 3 or 4% pyrite as anhedral blebs in the hematite-magnetite lenses and breccias. Traces of chalcopyrite(?) were seen in hand sample but were not found in thin sections. In the remainder of the Iron Range, sulphides were not seen in outcrop or hand sample but some thin sections have tiny blebs of pyrite (<100 μm) within quartz veins. Some pyritic quartz veins with silicic alteration halos occur near the Iron Range fault; their orientations are oblique to the fault. Also, a short distance to the east of the fault on the northern part of Iron Range Mountain, there is an old pit with sulphide-bearing (pyrite-chalcopyrite-galena) quartz vein material in its dump (David Wiklund, Creston, personal communication, 1994). These veins may be related to the pyrite occurrences within the fault.

Foliated gabbro occupies much the width of the fault zone. Mineralization within the gabbro consists of some massive hematite lenses, foliation-parallel veins and zones of disseminated hematite and magnetite, rarer crosscutting breccia veins, and a background level of about 0.5 to 1% disseminated magnetite. The gabbro - iron oxide lens contacts are typically covered by overburden. Where exposed, there are zones of bleaching (albitite?) up to 30 centimetres wide and quartz veins lining the contacts. Crosscutting breccia veins were observed along the margins of the fault zone where strongly foliated gabbro grades into unsheared gabbro of the Moyie sills. The veins are very irregular and contain angular fragments of altered gabbro in a hematitic matrix. Some breccia veins are spatially associated with irregular zones of crosscutting albitic alteration. Disseminated magnetite is ubiquitous in the sheared gabbro, sufficient to be easily detected with a hand magnet. Most of the Moyie sills in the area do not attract a hand magnet and do not register on the regional aeromagnetic map.

Late, white quartz veins cut across all other rock types. The veins are several millimetres to several centimetres wide and most are parallel to the trend of the fault zone. Quartz growth is generally in the plane of the veins and some have several centimetres of shear movement. Some veins contain hematite crystals or angular fragments of massive hematite, apparently plucked from older veins and lenses. Magnetite is present in some quartz veins. These veins are interpreted as having been emplaced late in the deformational history of the fault, representing the last effects of the Iron Range hydrothermal system.

Photo 2. Hematite-filled breccia veins cutting albitite. The veins are parallel to the fault zone. Hematite fillings and veins are interpreted to postdate the initial brecciation. (PST94-I.R.23)

LA GRANDE ZONE

The La Grande zone is the segment of the Iron Range fault in the detailed study area south of the main zone (corresponding to MINFILE 082SE021-028). There the fault zone runs about 250 metres east of the ridge top and is not trenched; it is only exposed where it crosses side ridges. The fault zone appears to be 20 to 40 metres wide but the full width is not exposed. The fault in this area is a zone of quartz veining with variable iron oxide content in a more diffuse zone of grey quartz-hematite alteration. Iron content locally reaches grades approaching that of the massive lenses in the main deposit but over narrower widths (<1 m). This quartz-hematite mineralization is crosscut by late white quartz veins, as in the main deposit. In the La Grande zone the late veins are more common but are less often characterized by shear textures. Locally these veins contain up to 4% hematite, sometimes as 1 to 2-millimetre, platy euhedra.

MOUNT THOMPSON ZONE

South of Highway 3, a magnetite-rich zone crops out on a ridge top approximately 1.5 kilometres south-southeast of Mount Thompson. A zone of albitite,1 to 2 metres wide, with disseminated to semimassive magnetite, cuts north-south through nearly flat-lying sediments. A wider surrounding zone has irregular hematite-filled fractures. In this area the fault changes from a single wide zone, as on Iron Range Mountain, to an anastamosing set of faults that are locally intruded by gabbro dikes. The individual faults are difficult to trace southward as outcrop becomes very scarce.

CRACKERJACK FAULT

A fault to the east of the main zone (Crackerjack fault; inset map in Figure 1) has a narrow zone (>5 m wide) of hematite-albitite breccia in one location, immediately to the north of Crackerjack Creek (Dean Barron, personal communication, 1994). One grab sample of the richest mineralization assayed 34% Fe_2O_3. The width of this zone and its extent along the fault are unknown due to poor exposure.

ALTERATION

Several alteration types are associated with the Iron Range deposit. Albite alteration is associated with the highest iron grades. In the main deposit, fine-grained, sugary albite alteration extends over most of the width of the fault zone. Albite alteration is confined to the fault

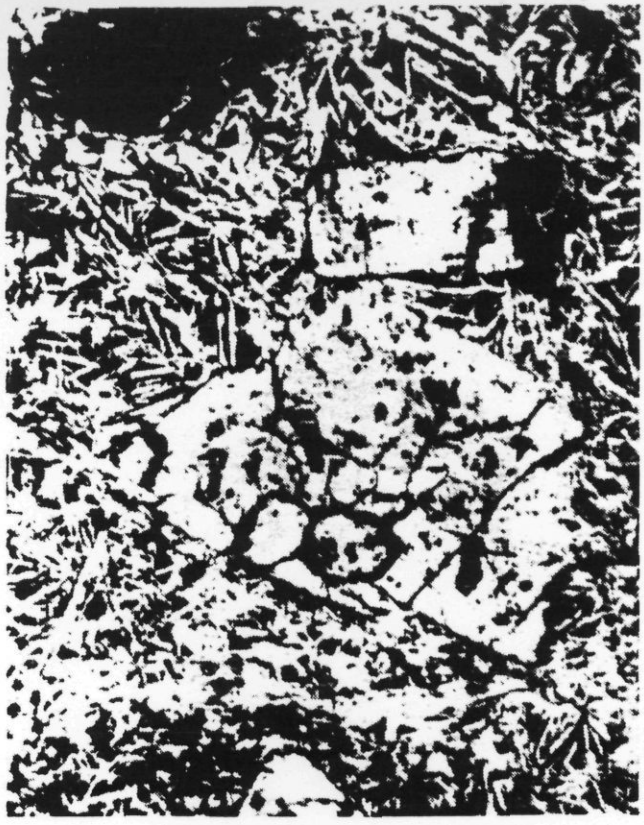

Photo 3. Photomicrograph showing euhedral magnetite grains in a matrix of bladed hematite. The magnetite grains are almost entirely pseudomorphed by hematite. The slightly darker core of the larger grain is residual magnetite. The field of view is approximately 0.75 by 1.25 mm. Reflected light, plane polarized. (PST94-I.R.11)

zone, except for rare apophyses which extend 1 to 2 metres into poorly foliated gabbro at the eastern contact of the main deposit. Although this alteration primarily affects sedimentary rocks in the fault zone, it is locally well developed in gabbro and, over the length of the fault, is only strongly developed near gabbro. Elsewhere early alteration in the fault zone is silicic.

Gabbro bodies within the fault zone are strongly foliated parallel to strike and are characterized by very strong chlorite alteration formed prior to, or during, shearing. The deformation fabric, seen in thin section, has porphyroclasts of plagioclase wrapped in fine-grained, commonly foliated chlorite. Weak S-C fabrics (Lister and Snoke, 1984) in foliated chlorite indicate west-side-down dip-slip movement. This contrasts with the completely brittle deformation of the albitite and may be attributable to the different competencies and response to stress of the lithologies during deformation. Locally the gabbro is bleached white by albitic alteration.

Sericitic alteration extends outward from the fault zone for about 500 to 1000 metres. The sericitic overprint is best developed in silty beds and is associated with the locally well developed cleavage. In addition to sericite, irregular veins and knots of quartz, epidote, and chlorite were observed in several outcrops of sandstone 100 metres to west of the trenches on the X-ray claim. Sericitic alteration was noted in only one locality in the fault zone, at its western edge on the Maple Leaf claim. There it is associated with a very strong, slaty cleavage developed parallel to the fault. This sericitic slate encloses the westernmost massive hematite lens (Figure 2).

Other alteration associated with the Iron Range fault is minor. Weak, rusty surface stain is present throughout the area, but this is a regional characteristic of the middle and upper Aldridge rocks, due to ubiquitous disseminated pyrrhotite (Höy, 1993). Mafic minerals within the gabbro sills near the fault zone have some chlorite overprint, but it is much weaker than within the fault zone.

Away from the parts of the Iron Range fault and subsidiary faults which have significant iron mineralization in surface exposures, the faults are characterized by a zone of cataclasis and silicic and/or albitic alteration 10 to 20 metres wide. Chloritic alteration was noted in several locations, all near intersections with Moyie sills. Examples are near the International Boundary, and on two faults on the northeast flank of Iron Range Mountain (in 82F/8).

PARAGENESIS AND RELATIONSHIP OF MINERALIZATION TO DEFORMATION

The origin of the Iron Range deposits is strongly linked to deformation in the Iron Range fault zone. Deformation can be separated into three episodes which may represent three stages of a continuous deformation. These are related to different stages in the evolution of the iron oxide mineralization. This is summarized in a paragenetic diagram (Figure 3).

The timing of the first movements on the Iron Range fault is difficult to determine. It is possible that it was originally a growth fault and served as a conduit for feeder dikes to the Moyie sills. The basis for this interpretation is the thick accumulation of sills in this part of the basin (Brown and Stinson, 1995, this volume). Also, much of the deformed material in the fault zone is gabbro, forming long narrow bodies. These have been interpreted as dikes (Blakemore, 1902; Langley, 1922; Young and Uglow, 1926). Within the main deposit, however, at least some of the gabbro bodies are sills that have been stretched into the plane of the fault zone, forming large drag folds and possibly sheath folds (Figure 2). The apparent thickening of the sills near the fault in the detail map area is mainly an effect of topography, but may be partly due to minor shearing along the margins of the main fault zone. If the sheared gabbros are deformed sills, then motion on the Iron Range fault probably began well after the deposition and burial of the Aldridge Formation. Pre-mineralization movement on the fault is inferred from the initial localization of albitite alteration along a narrow, crosscutting zone in the Aldridge sediments.

Albite alteration in the Aldridge Formation is usually the result of hydrothermal activity related to the intrusion of Moyie sills into relatively unconsolidated, water-saturated sediments at shallow levels below the sea-floor (Höy, 1993). The very strong albite alteration in

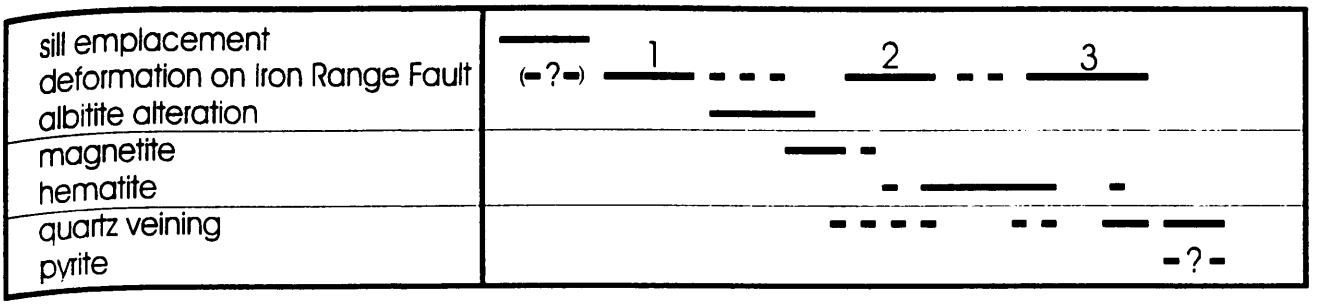

Figure 3. Diagram illustrating paragenetic sequence for the Iron Range deposit. Numbers refer to deformational episodes: (1) Initiation of the Iron Range fault and formation of hydrothermal conduit; (2) Cataclasis of albitite and shearing of gabbro; (3) Further cataclasis and shearing of iron ore.

the main Iron Range deposit is confined to the fault zone, although it is only developed in and around gabbro bodies. Initial magnetite mineralization is interpreted to have occurred with the albitic alteration, perhaps late in this episode. This mineralization is only well developed where subsequent brecciation is weak and shear fabrics are lacking. Magnetite precipitation continued into the next recognizable stage in the evolution of the Iron Range fault.

The main deformation episode followed the albite alteration. In the wide fault zone this consisted of extensive cataclastic brecciation of albitite, foliation development in gabbro, and local development of slaty cleavage in sericitized sediments. The albitite microbreccias are cataclasite (>50% matrix), the breccias are protocataclasite (<50% matrix), and gabbro within the fault zone is locally mylonitic, according to the definitions of Sibson (1977). This variation in deformational style between the different lithologies indicates that this episode occurred at several kilometres depth; cataclastic deformation can occur at depths up to about 5 kilometres (Ramsay and Huber, 1987, p. 584)

This deformation acted as ground preparation for hematite mineralization, although these events may have overlapped to some extent. Fine-grained hematite formed large, fault-parallel lenses and replaced fault gouge in the breccias. This episode began with magnetite deposition, but hematite replaced magnetite and is far more abundant. This change indicates that the fluids became increasingly oxidizing early in this main stage of iron mineralization.

Deformation continued after the main mineralizing episode, resulting in the formation of fractures, shear veins, and local ductile deformation of hematite-rich rocks. Quartz-filled shear veins, with vein-parallel mineral growth and offsets across them, are common along the length of the fault. They crosscut all other lithologies, including early silicified rocks in the La Grande area. Rare extension veins with mineral growth perpendicular to the vein walls were also observed. These vein textures resemble the vein associations in mesothermal, shear zone hosted gold deposits (Roberts, 1987), and may have formed in similar conditions. The iron oxide content of these veins is low. Local, well developed S-C fabrics in hematite breccias are associated with shear veins. Locally, hematite veins are brecciated and filled by quartz. Sulphide-bearing quartz veins, although not shear veins, may have been emplaced during this stage in the deposit evolution or they may be later and unrelated to the iron oxide mineralization.

The deformation style and alteration of the Iron Range fault and subsidiary faults is unusual compared to other faults in the surrounding area (Brown and Stinson, 1995, this volume). These characteristics, and the possible connection to the Moyie sills, indicate that the fault is old, maybe Proterozoic, and perhaps contemporaneous with early movements on the Moyie and St. Mary faults. The source of the large volume of iron contained in the Iron Range deposit is unknown. Potential sources include the Moyie sills and the basement of the Aldridge Formation.

COMPARISON TO OTHER MINERAL DEPOSITS

Hydrothermal iron deposits have received particular attention over the last few years, mainly due to the results of recent work on the Olympic Dam deposit in Australia. Early studies of the Olympic Dam, based on limited drilling information, interpreted the deposit as sedimentary breccias with mineralization and alteration largely due to diagenetic processes (Roberts and Hudson, 1983). Recent studies, based on extensive core logging and underground mapping, have established the hydrothermal nature of the breccias and described the evidence for near-surface hydrothermal brecciation within the host granitic batholith (Oreskes and Einaudi, 1990; Reeve *et al.*, 1990). Copper, gold, silver, uranium, and rare earth elements were deposited late in the evolution of the breccias, after significant iron metasomatism, and were enriched by supergene processes (Oreskes and Einaudi, 1990). These studies note that the core zone of the breccias is broadly associated with a topographic lineament which may reflect an underlying fault zone.

Recent studies propose that the Olympic Dam deposit has important similarities with certain other mineral deposits. This has resulted in the definition of a class of deposits; Olympic Dam type, or Proterozoic iron oxide , (Cu-U-Au-REE; Hitzman *et al.*, 1992;

Lefebure, 1995, this volume). Canadian deposits included in this classification by these workers include the Wernecke breccias in Yukon Territory and deposits of the Great Bear magmatic zone in the Northwest Territories. One aspect of the deposit class is the alteration zoning, a summary of which is presented by Hitzman *et al.* (1992). They propose a typical pattern of albite-magnetite-actinolite grading upward and outward through a potassic zone to an outer hematite-sericite zone, with an intermediate zone of albite-sericite-magnetite alteration in sediment-hosted deposits. The Iron Range has an inner core zone of albite alteration and an outer envelope of sericite alteration corresponding to the deeper sodic alteration zone of this deposit class.

The Iron Range deposit has similarities to this broad class of mineral deposits and could reasonably be included in it. With respect to the Olympic Dam iron breccias, the main genetic differences appear to be the structural style, the origin of the brecciated hostrocks, and the greater depth of formation of the Iron Range deposit. However, enrichment in base and precious metals at Olympic Dam do not have a demonstrated corollary at Iron Range. It is interesting to note the possible fault control at depth at Olympic Dam (Oreskes and Einaudi, 1990), and to speculate that if this fault, or fault system, controlled the upward migration of hydrothermal fluids and metals, it might resemble the present level of exposure on Iron Range Mountain.

ACKNOWLEDGMENTS

We thank Dean Barron and Gavin Manson for assistance in the field. Discussions with Paul Ransom and David Lefebure were useful. The manuscript was greatly improved by critical reviews by Kirk Hancock and John Newell.

REFERENCES

Blakemore, M.E. (1902): The Iron Ore Deposits near Kitchener, B.C.; *Journal of the Canadian Mining Institute*, Volume 5, pages 75-81.

Brown, D.A. and Stinson, P. (1995): Geologic Mapping of the Yahk Map Area, Southeastern British Columbia (82F/1): An update; *in* Geological Fieldwork 1994, Grant, B. and Newell, J.M., Editors, *B.C. Ministry of Energy, Mines and Petroleum Resources*, Paper 1995-1, this volume.

Geological Survey of Canada (1971): Aeromagnetic Map 8471G, Yahk, British Columbia (NTS 82F/1); *Geological Survey of Canada* and *B.C. Ministry of Energy, Mines and Petroleum Resources*.

Hitzman, M.W., Oreskes, N. and Einaudi, M.T. (1992): Geological Characteristics and Tectonic Setting of Proterozoic Iron Oxide (Cu-U-Au-REE) Deposits; *Precambrian Research*, Volume 58, pages 1-47.

Höy, T. (1993): Geology of the Purcell Supergroup in the Fernie West-half Map Area, Southeastern British Columbia; *B.C. Ministry of Energy, Mines and Petroleum Resources*, Bulletin 84.

Langley, A.G. (1922): Kitchener Iron-deposits, Eastern District (No. 5); *in* Minister of Mines Annual Report 1921, *B.C. Ministry of Energy, Mines and Petroleum Resources*, pages G145-G149.

Lefebure, D.V. (1995): Two Intriguing Mineral Deposit Profiles for British Columbia; *in* Geological Fieldwork 1994, Grant, B. and Newell, J.M., Editors, *B.C. Ministry of Energy, Mines and Petroleum Resources*, Paper 1995-1, this volume.

Lister, G.S. and Snoke, A.W. (1984): S-C Mylonites; *Journal of Structural Geology*, Volume 6, pages 617-638.

Oreskes, N. and Einaudi, M.T. (1990): Origin of Rare Element-enriched Hematite Breccias at the Olympic Dam Cu-U-Au-Ag Deposit, Roxby Downs, South Australia; *Economic Geology*, Volume 85, pages 1-28.

Ramsay, J.G. and Huber, M.I. (1987): The Techniques of Modern Structural Geology, Volume 2: Folds and Fractures; *Academic Press*, 700 pages.

Reesor, J.E. (1981): Grassy Mountain, Kootenay Land District, British Columbia (82F/8); *Geological Survey of Canada*, Open File 820.

Reeve, J.S., Cross, K.C., Smith, R.N. and Oreskes, N. (1990): The Olympic Dam Copper-Uranuim-Gold-Silver Deposit, South Australia; *in* Geology of Mineral Deposits of Australia and Papua New Guinea, Hughes, F., Editor; *Australian Institute of Mining and Metallurgy*, Monograph 14, pages 1009-1035.

Roberts, D.E. and Hudson, G.R.T. (1983): The Olympic Dam Copper-Uranium-Gold-Silver Deposit, Roxby Downs, South Australia; *Economic Geology*, Volume 78, pages 799-822.

Roberts, R.G. (1987): Archean Lode Gold Deposits, *in* Ore Deposit Models; Roberts, R.G. and Sheahan, P.A., Editors, *Geological Association of Canada*, Geoscience Canada Reprint Series 3, pages 1-20.

Sibson, R.H. (1977): Fault Rocks and Fault Mechanisms; *Journal of the Geological Society of London*, Volume 133, pages 191-213.

Young, G.A. and Uglow, W.L. (1926): Iron Ores in Canada, Volume I, British Columbia and Yukon; *Geological Survey of Canada*, Economic Geology Series, No. 3, pages 132-142.

Appendix III

High Resolution Geophysical Survey Report

20. HIGH RESOLUTION GEOPHYSICAL SURVEY OF THE PURCELL BASIN AND SULLIVAN DEPOSIT: IMPLICATIONS FOR BEDROCK GEOLOGY AND MINERAL EXPLORATION

C. Lowe[1], D.A. Brown[2], M.E. Best[3], and R.B.K. Shives[4]

1. GSC - Pacific, Natural Resources Canada, P.O. Box 6000, 9860 West Saanich Road, Sidney, British Columbia, V8L 4B2
2. B.C. Geological Survey Branch, Ministry of Energy and Mines, 1810 Blanshard Street, Victoria, British Columbia, V8W 9N3
3. Bemex Consulting International, 5288 Cordova Bay Road, Victoria, British Columbia V8Y 2L4
4. Geological Survey of Canada, Mineral Resources Division, 601 Booth Street, Ottawa, Ontario, K1A OE8

ABSTRACT

8800 line-kilometres of high-resolution multi-parameter (electromagnetic, magnetic, gamma-ray spectrometry, and VLF) geophysical data were recently acquired in three survey areas in the Purcell Basin, southeastern British Columbia. One of the survey areas encompasses the world-class Sullivan Sedex deposit. The radiometric data provide the first Canadian survey of a Sedex deposit setting, and the electromagnetic data are the first such public-domain data for the region. The surveys were complemented by ground follow-up of selected anomalies and the measurement of physical properties of rocks on outcrops, hand and core specimens. Collectively, these data provide an opportunity to geophysically characterize the lithostratigraphy and Sedex mineralization within the survey areas.

The geophysical data are valuable to geological mapping and interpretation in the survey areas. Using the contrasting radiometric, magnetic and EM responses between the gabbroic Moyie sills and the sedimentary rocks in which they were emplaced, several new sill exposures have been recognized and new sill correlations facilitated. Radiometric and EM responses are particularly sensitive to the nature and content of phyllosilicate minerals, and allow the discrimination of different sedimentary units within the stratigraphic column, even in areas of thin till cover. Magnetic and radiometric data detect subtle variations within Cretaceous granitic intrusions. Faults in the Yahk area are anomalously magnetic, suggesting that fault structures, in addition to those of the Iron Range, were conduits for hydrothermal flow.

Known sulphide mineralization and hydrothermal alteration in the Sullivan - North Star Corridor correlate with enhanced bedrock conductivity, strong finite conductors and positive magnetic anomalies. Sericitic alteration, which is spatially associated with the sulphide mineralization, is imaged in the radiometric data as elevated potassium levels and depleted thorium:potassium ratios relative to unmineralized host rocks. The integrated patterns permit formulation of exploration criteria for undiscovered Sedex occurrences elsewhere in the basin. However, exploration strategies should consider the limitations of the maximum crustal depth to which the different geophysical methods can detect a response: about 30 cm for the radiometric method; about 100 m for the EM method; and up to 20 km for the magnetic method.

INTRODUCTION

In 1995 and 1996 approximately 8800 line-kilometers of electromagnetic, total field magnetic, gamma-ray spectrometric and VLF data were acquired in three survey areas of the Purcell anticlinorium, southeastern British Columbia. The surveys, conducted by Dighem I-Power, were government-funded and specifically designed to cover the Aldridge Formation that hosts the most significant mineral deposits of the area (Fig. 20-1). The northern (Fig. 20-1, Area 2, Findlay Creek) survey area covers about 400 km^2 south of Findlay Creek, and west of Canal Flats. The central (Fig. 20-1, Area 1, St. Mary River) survey area covers approximately 2000 km^2 extending from 6 km east of Kootenay Lake to about 7 km east of the town of Kimberley and includes the Sullivan Mine. The southern (Fig. 20-1, Area 3, Yahk) survey area comprises about 600 km^2 and extends east from Creston to Yahk and south to the U.S. border. The surveys were conducted using an Aerospatiale (AS350B1) helicopter flown at a mean terrain clearance of 60 m (Fig. 20-2). Flight lines, oriented east-west in the St. Mary River and Yahk survey areas and northwest-southeast in the Findlay Creek area, were spaced 400 m apart with control lines approximately 5 km apart.

A number of published reports describe the data, and examine their utility for regional geology and mineral exploration studies (Brown et al., 1997; Lowe et al., 1997, 1998). In this summary paper we present brief explanations of each of the geophysical methods used and comment on their capabilities and limitations. We describe the expected, as well as the observed, geophysical responses of the lithologies and the known mineral occurrences of surveyed areas and we also discuss the geological implications of observed variations. We focus on the Sullivan-North Star Corridor, which includes the Sullivan and the small North Star and Stemwinder Pb-Zn-Ag deposits. Growth faults, chaotic breccia, Moyie sills, manganiferous garnet-rich beds and muscovite and albite-biotite-chlorite alteration are associated with the mineralization in this corridor (Turner et al., 2000a and b). We consider the geophysical responses of each of these features, relying not only on observed correlations among the various parameters, but also on measurements conducted on rock samples.

Lowe, C., Brown, D.A., Best, M.E., and Shives, R.B.K.
2000: High Resolution Geophysical Survey of the Purcell Basin and Sullivan Deposit: Implications for Bedrock Geology and Mineral Exploration; in The Geological Environment of the Sullivan Deposit, British Columbia, (ed.) J.W. Lydon, J.F. Slack, T. Höy, and M.E. Knapp; Geological Association of Canada, Mineral Deposits Division, MDD Special Volume No. 1, p.

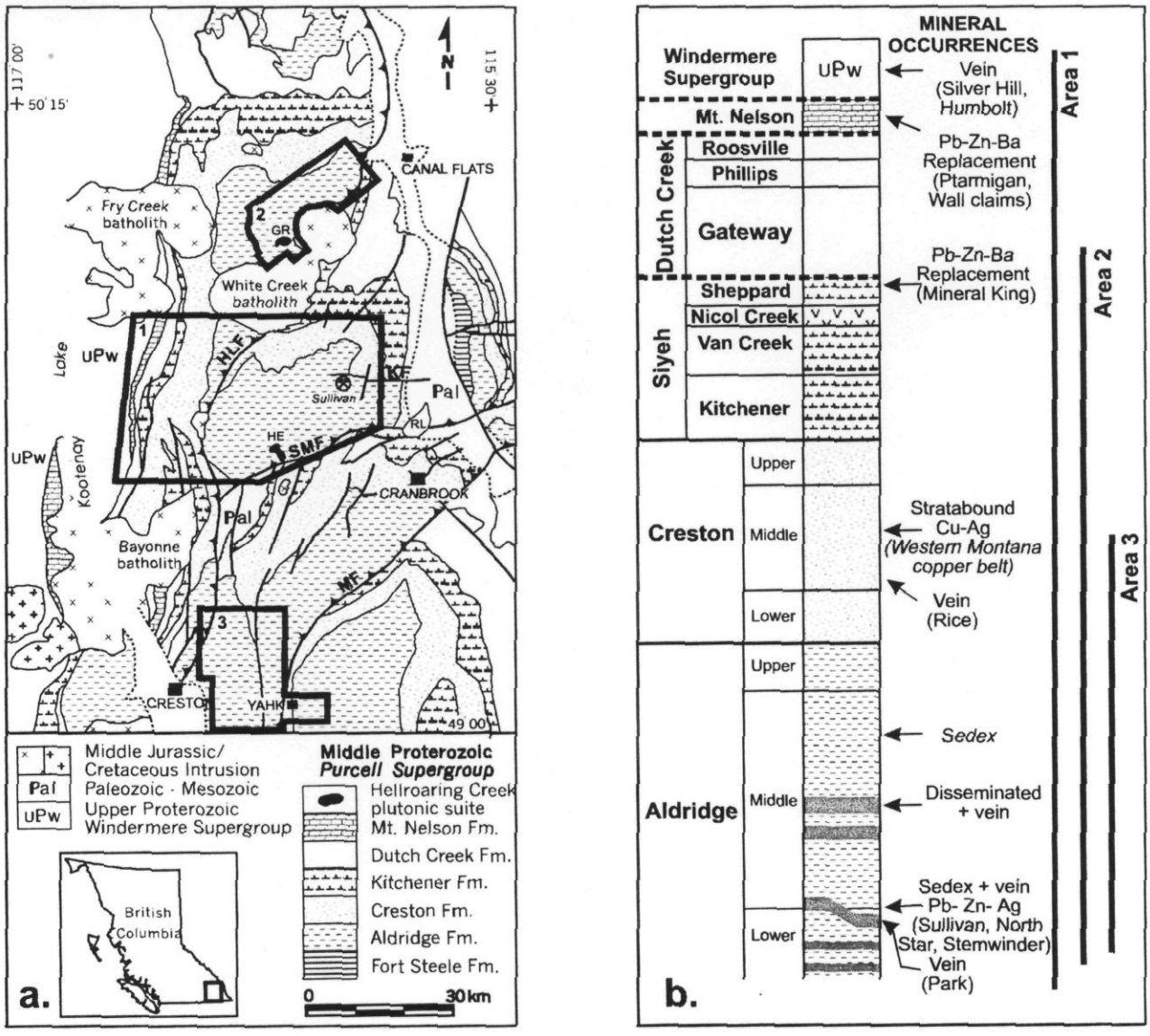

Figure 20-1. **(a)** Regional geological setting of Purcell Supergroup showing the location of the three geophysical survey areas within the *Purcell anticlinorium (modified from Höy et al., 1995). 1 = St. Mary River area; 2 = Findlay Creek area; 3 = Yahk area.* GR = Greenland Creek stock, HE = Hellroaring Creek stock, HLF = Hall Lake fault, KF = Kimberley fault, MF = Moyie fault, RL = Reade Lake pluton, SMF = St. Mary fault. **(b)** Stratigraphic column for the Purcell Supergroup and basal Windermere Supergroup (modified from T. Höy, written comm., 1996). The stratigraphic position of several mineral occurrences are indicated. Thick vertical lines denote the range of stratigraphy exposed in each survey area.

GEOLOGICAL SETTING

Only a brief overview of the geology of the survey areas is given here. More thorough descriptions are provided by Höy et al. (2000) and by Leech (1957); Reesor (1958, 1973); Höy (1984a, b, 1993); and Brown et al. (1995). The three survey areas lie within the Purcell anticlinorium, a broad north-plunging structural culmination cored by middle Proterozoic (circa 1500 to 1350 Ma) metasedimentary rocks of the Purcell Supergroup (Fig. 20-1). The succession is more than 12 km thick and comprises syn-rift, deep water turbidites of the Aldridge Formation, and overlying shallow-water to locally subaerial clastic, carbonate rocks and minor volcanic rocks of the Creston and younger formations which form late- and/or post-rift sedimentary sequences (*see* Fig. 20-1b). Laterally extensive gabbroic sills ("Moyie sills") intrude the Aldridge sedimentary rocks and provide a minimum age for the syn-rift package (1468 Ma, D.W. Davis, unpub. data) (Anderson and Davis, 1995). Upper Proterozoic conglomeratic, siliciclastic and volcanic rocks of the Windermere Supergroup unconformably overlie Purcell Supergroup rocks.

The Sullivan deposit and several smaller Pb-Zn occurrences of probable sea-floor genesis occur near the contact between the lower and middle members of the Aldridge Formation. The majority of other similar base metal and/or tourmaline occurrences occur near the middle part of the

middle member of the Aldridge Formation (Höy et al., 2000). The three survey areas were therefore selected primarily to acquire geophysical signatures from the Sullivan deposit and the Sullivan Corridor and to maximize coverage of the Aldridge Formation. However, in addition the survey areas were also designed to acquire geophysical signatures from representatives of most other lithologies of the Purcell anticlinorium. Thus, although turbidites of the Aldridge Formation and siltstones, quartzites and argillites of the overlying Creston Formation predominate in the survey areas, sedimentary rocks of the upper part of the Purcell Supergroup (Kitchener Formation through to the Mount Nelson Formation) and the unconformably overlying Windermere Supergroup (Fig. 20-1b) are covered in the western part of the St. Mary River area. Proterozoic granitic stocks, that appear to have been preferentially generated along the rift axis, are represented by the Hellroaring Creek stock (4 km^2) in the St. Mary survey area and by the Greenland Creek pluton (1.6 km^2; Reesor, 1996) in the Findlay Creek survey area. Small outliers of Paleozoic shelf sediments occur in the southern part of the St. Mary area, and Cretaceous granitic batholiths are represented by the White Creek and Fry Creek batholiths in the St. Mary and Findlay survey areas, respectively.

GEOPHYSICAL METHODS

The full set of geophysical images acquired by the survey has been published as a set of eighteen 1:50,000 images (British Columbia Ministry of Employment and Investment, 1996). The purpose of this paper is to describe the principals of the geophysical methods used in the survey and to discuss the different geophysical responses in the context of the geological characteristics of rocks of the Purcell anticlinorium. Within the constraints of this publication, it is not possible to illustrate all of the geological and geophysical correlations described below, readers wishing to do so are encouraged to consult the 1:50,000 images.

Electromagnetics

Principles and methodology

Electromagnetic (EM) methods are inductive techniques based on Faraday's Law. They measure conductivity (or its inverse, resistivity) and are used to map its variation at the earth's surface. A transmitter, consisting of a time-varying current circulating in a multi-turn coil, produces electric and magnetic (EM) fields that induce time-dependent eddy currents within conductors. In turn, these eddy currents generate secondary EM fields. The objective of an EM survey is to measure the secondary fields, and from these measurements, deduce the electrical properties of the earth's subsurface (Keller and Frischknect, 1966; Nabighian, 1994). Two types of airborne EM (AEM) systems are available. Time-domain EM systems employ a transmitter current consisting of a current pulse or set of current pulses (for example the GEOTEM system). The secondary magnetic fields generated with a time-domain system are measured by one or more receiving coils at several different times. Frequency-domain EM systems employ a transmitter current consisting of a continuous or sinusoidal current at one or more frequencies.

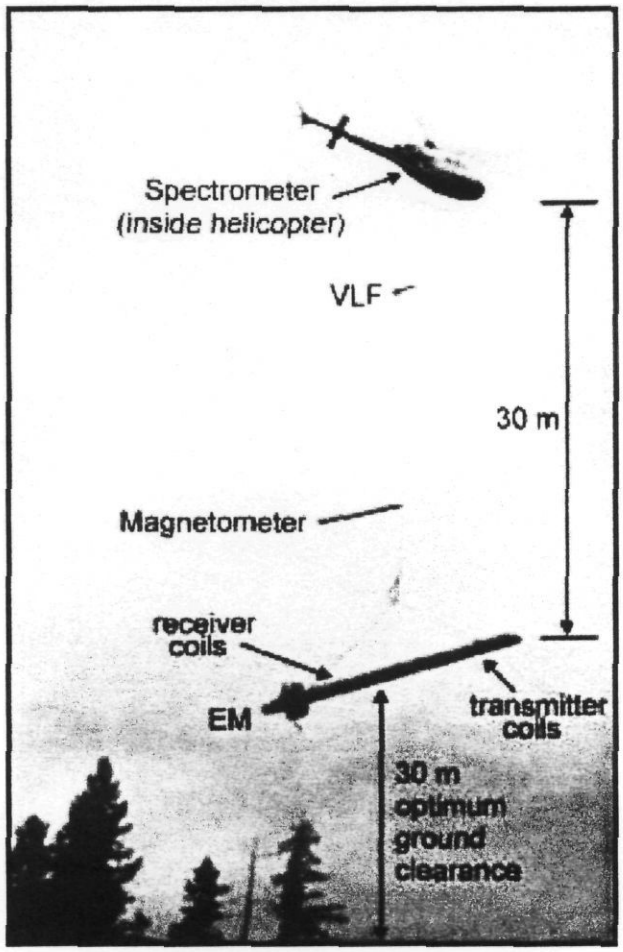

Figure 20-2. Photograph of the Aerospatiale helicopter used to conduct the survey. The helicopter was flown at a mean terrain clearance of 60 m. The gamma-ray spectrometer is housed inside the body of the helicopter, and the VLF, magnetic and electromagnetic systems are housed in birds 10 m, 20 m and 30 m, respectively, beneath the helicopter.

The secondary magnetic fields generated at each frequency with a frequency-domain system are measured by one or more receiving coils. An in-phase component, in-phase with the transmitted sine wave current, and a quadrature component, ninety degrees out of phase with the transmitted sine wave current, are measured at each frequency. These values are *normalized* by dividing them by the in-phase value that would be measured in the absence of any conducting bodies (empty space).

The Dighem airborne EM system used in this survey is a frequency-domain EM system consisting of two vertical coaxial transmitter-receiver coil pairs with frequencies of 900 Hz and 5500 Hz, respectively, and three horizontal coplanar transmitter-receiver pairs with frequencies of 900 Hz, 7200 Hz and 56,000 Hz, respectively. The spacing between coil pairs is 8 m except for the 56,000 Hz, which is 6.3 m. All these coils are contained in a fibreglass bird that was towed beneath the helicopter 30 m above the ground surface (Fig. 20-2). The magnitudes of the in-phase and quadrature (secondary) fields depend on coil orientation and separation, transmitter frequency, and the conductivity of the

earth. The Dighem coil orientations (coplanar and coaxial) and frequencies are chosen to cover as wide a range of conductor responses as possible for coil separations of approximately 8 m. Generally, the in-phase signal saturates (i.e. attains a constant value) at high frequencies and/or large conductivity values, whereas the quadrature signal attains a maximum value at a finite frequency that depends on the subsurface conductivity and the coil orientation and spacing.

The "skin depth", or depth of penetration of an EM system also depends on the frequency of the system and the conductivity of the earth, with depth of penetration increasing as frequency or conductivity decreases. Consequently, the 900 Hz frequency provides information on the deepest conductivity distribution of the earth, while the 56,000 Hz penetrates only the shallow subsurface. The orientation of the coils determines how the transmitted field couples to a conductive body. Flat lying bodies, such as overburden or sills, couple to the horizontal coplanar coils more effectively than to the vertical coaxial coils. On the other hand, vertical conductors, such as dykes, couple more effectively to the vertical coaxial coils. The size, shape and conductivity of a finite conducting body determine the depth to which it can be "seen" with an EM system (i.e. has secondary field responses that are measurable). The exact behavior is quite complex, but with the low frequency of 900 Hz and coil separation of 8 m of the Dighem system, the maximum depth of penetration is approximately 100 m.

Electromagnetic responses in the Purcell Basin

The conductivity of a rock depends on the minerals present within the rock and on the amount and chemical composition of the pore fluid. Bulk conductivity of low porosity rocks such as volcanic, plutonic, metamorphic and older sedimentary rocks depends more on conducting minerals than on pore fluid. Minerals that can increase the conductivity of a rock include sulphides, clays and graphite. The effect a mineral has on the conductivity of a rock depends on the amount of the mineral present and the connectivity of the mineral grains. A few percent (less than 5%) pyrite or pyrrhotite dispersed throughout a rock may or may not increase the bulk conductivity. It depends on whether the grains are touching each other to form a continuous path for current to flow. The bulk conductivity of a rock with less than 5% sulphides, or any other conducting mineral, is nearly the same as a rock without sulphides. As the proportion of conducting minerals increases the opportunity for mineral grains to touch (connect) increases, hence the bulk conductivity may increase as well. However, even massive sulphide deposits with more than 30% sulphides may be poor conductors if the sulphide grains are coated with a non-conducting mineral (Palacky, 1987).

No laboratory or in situ resistivity measurements were made on rocks in the survey areas. Typical resistivity ranges for sediments comparable to those exposed in the survey areas are (Palacky, 1987): argillite, 70 to 850 ohm-m (14 to 1.2 mS/m; note S/m is the unit of conductivity and is the reciprocal of resistivity which has a unit of ohm-m); dolomite, 700 to 2500 ohm-m (1.4 to 0.4 mS/m); limestone, 350 to 6000 ohm-m (2.9 to 0.16 mS/m); and sandstone, 1000 to 4000 ohm-m (1 to 0.25 mS/m). The resistivity of mudstone and siltstone can vary depending on the graphite and clay content (the greater the graphite and/or clay content, the lower the resistivity). Volcanic and plutonic rocks have resistivity values generally greater than 1000 ohm-m (1 mS/m) and often greater than 5000 ohm-m (0.2 mS/m).

Apparent conductivity is estimated at each location by assuming the earth is a homogeneous conductor and solving for the conductivity (Fraser, 1975). The in-phase and quadrature values, for a given frequency and coil pair, can be used to estimate the conductivity of a homogenous earth because the height of the transmitter and receiver coil pair above the earth are known from the radar altimeter. Obviously the estimated conductivity values near the boundary between two rock units with different conductivities or near finite conducting bodies can be distorted from their actual value; hence the name *apparent conductivity*. Coplanar coil pairs generally produce more representative apparent conductivity maps than coaxial coil pairs for reasons of coupling discussed earlier. Apparent conductivity maps generated from the 900 Hz coplanar pair measure the average conductivity of the earth to a depth of 100 m or more whereas the 56,000 Hz coplanar coil pair only measures the top few meters.

Consequently, argillite in the Aldridge Formation, argillite and argillaceous dolomitic units within the Creston, Kitchener, and Mount Nelson formations, as well as graphitic horizons throughout the stratigraphic sections are expected to show up as conductive zones on apparent conductivity maps. Thick, clay-rich surficial sediments, such as those along many of the river valleys within the survey areas, are also expected to be conductive. Igneous intrusions (e.g. Hellroaring Creek stock; the White Creek and Fry Creek batholiths; Moyie sills) generally do not contain a significantly high proportion of conductive minerals and generally have low porosities, and would thus be anticipated to correlate with resistive zones on apparent conductivity maps. Volcanic rocks (e.g. Nicol Creek lavas in the southeastern St. Mary River area) are also typically resistive, however these rocks tend to have higher porosities, and this may lower their resistivity somewhat.

Finite bedrock conductors are usually caused by massive sulphide or graphite bodies. Shear zones, faults and fractures can also behave like finite bedrock conductors where they contain conducting minerals generated by hydrothermal alteration. A unique source for a finite bedrock conductor is not easy to determine since all generate similar EM responses. Indirect indicators, such as the location of a conductor relative to known geology, the shape of the EM response and the conductivity-thickness product of the conductor, are used to discriminate between different types of bedrock conductors. Surficial conductors commonly produce EM responses quite similar in appearance to those generated by bedrock conductors. However, they can usually be distinguished from bedrock conductors as they are generally less conductive and, by their nature, shallower. Consequently surficial conductors can be distinguished by using different frequencies to determine the depth to the top of the conductor and their conductivity-thickness product.

The apparent conductivity maps, particularly the 900 Hz (Fig. C20-3) and 7200 Hz coplanar maps, outline both resis-

tive and conductive zones within the survey areas that can be correlated with known bedrock geology. Examples of the sensitivity of the method to clay and graphite content within sedimentary units are numerous. An approximately north-trending conductive zone in the Yahk survey area (Fig. C20-3c) west of the Carroll Fault within the Middle and Upper Aldridge Formation has conductivities between 3 and 20 mS/m (333 to 50 ohm-m). This conductive zone is approximately 2 to 3 km wide and extends the length of the survey area. It corresponds with graphitic mudstones and carbonaceous argillites. Similar zones, straddling the contact between the Lower and Middle Aldridge Formation occur within the Saint Mary River survey area, e.g. one near the Vulcan mineral occurrence (Fig. C20-3a). The origin of the Vulcan zone, which extends southwestward from the mineral occurrence, is not yet established. It is narrower than that in the Yahk area, and it has lower conductivities (between 4 and 100 mS/m; 250 and 10 ohm-m).

Within the Saint Mary River area, the Creston Formation (mPc) is generally resistive (Fig. C20-3a) corresponding with the predominance of arenaceous units. Where the proportion of argillites increases so too do the conductivities. For example, the NNE-trending conductive (1.5 to 10 mS/m; 667 to 100 ohm-m) horizon which extends south-southwestward from 116° 26' in the north to about the middle latitude of the survey area correlates with mapped argillaceous units in the lower Creston Formation (Fig. C20-3a).

A NNE-trending conductive (40 to 200 mS/m; 25 to 5 ohm-m) zone in the northwest portion of the Saint Mary River survey area (Fig. C20-3a) is about 3 km wide and correlates with mapped exposures of argillite in the upper Proterozoic Horsethief Creek Group. A large number of finite conductors were delineated within this conductive zone using the 900 Hz coaxial coil data. The conductors are thought to be caused by graphite-rich bodies within the argillite. Farther to the south where quartzite predominates in this formation, apparent conductivities are much lower and only a few weak conductors are delineated. Conductive zones within the Dutch Creek (mPdc), Kitchener (mPk) and Mount Nelson (mPmn) formations in the northwest corner of the St. Mary survey area appear to correspond to argillaceous sequences.

In general, the southwestern portion of the Saint Mary survey area is less conductive than the northwestern portion, even though the same formations have been mapped in both regions. This implies that the southern portion is less argillaceous and more quartzitic than the northern portion. The Dutch Creek Formation near the southern boundary of the survey area shows up as a conductive zone and has conductivities similar to those in the northwest corner. There are several weak conductors (conductivity-thickness between 1 and 5 S) associated with this latter zone.

Conductive zones are observed over several of the river valleys, including the St. Mary River and Matthew Creek in the St. Mary survey area and the Goat River and Kitchener Creek in the Yahk survey area (Fig. C20-3a, c). These zones are presumably due to clay-rich surficial deposits. They overprint the underlying bedrock geology making interpretation difficult. Man-made conductors related to mine tailings in the Sullivan area also overprint the bedrock geology.

Many of the Cretaceous intrusions are difficult to recognize on the apparent resistivity maps because they are resistive zones in a resistive background. For example, the Hall Lake and Sawyer Creek stocks in the Saint Mary survey area (Fig. C20-3a). Similarly, gabbroic Moyie sills in all three survey areas often cannot be distinguished by their electromagnetic responses. However, where sills intrude conductive units, such as graphitic mudstones and carbonaceous argillites in the Middle Aldridge Formation, southern Yahk survey area (Fig. C20-3c) they are readily distinguished.

Most of the faults in the survey areas are not imaged on apparent conductivity maps. This is true even in the case of the Carroll Fault (Fig. C20-3c) where an apparent conductivity contrast is observed across this fault. The contrast is fortuitous, due to the presence of graphitic units in the Middle Aldridge Formation to the west of the fault only and not to the presence of conductive material in the fault zone itself. Fine-grained, clay-rich gouge comprises the matrix of many large tabular breccia bodies mapped in the Iron Range Fault zone (Stinson and Brown, 1995), yet this fault is not imaged electromagnetically. Several finite conductors are mapped along or proximal to the trace of this fault, although most are quite weak (<5 S), or are cultural in origin (e.g. the power line in the Goat River Valley). Stinson and Brown (1995) observed that in the northern part of Iron Range Mountain up to 3-4% pyrite occurs in the fault zone but elsewhere sulphide minerals are rare. The lack of EM response suggests that where pyrite does exist it must have poor electrical connectivity.

Several narrow bedrock conductors located near the Vulcan prospect (Fig. C20-3a) have moderate conductance (5 to 20 S). Some of these conductors were also detected by ground UTEM surveys (Webber, 1979) and subsequently drilled. One hole encountered pyrrhotite in laminations and disseminated in smaller patches at depths of 85 to 95 m (Webber, 1979). Another drill hole encountered disseminated and massive pyrrhotite zones locally containing magnetite at depths of 40 to 45 m (Anderson, 1985). Non-cultural finite conductors aligned across adjacent flight lines are recognized near the Leadville Mine in the northern part of the Yahk survey area and elsewhere. Disseminated sulphide mineralization or clay-rich alteration products developed in shear zones are possible explanations of these aligned conductors.

Magnetics

Principles and methodology

The Earth's magnetic field (the *Geomagnetic* field) comprises three parts: (1) The *internal* field, varies very slowly in time, is of internal origin, and is thought to be due to the movement of partially molten iron in the outer core; (2) The *external* field, which is very small compared to the internal field, is mainly due to solar activity and may vary rapidly in time; (3) Spatial variations of the internal field, which are usually small, and nearly constant in time and space. These are caused by contrasts in the magnetic properties of near-surface rocks and referred to as *local magnetic anomalies*. They are of particular interest to geoscientists and explorationists.

Magnetometers measure all three components of the geomagnetic field. Because the internal field changes slowly over time, models of this field, called the International Geomagnetic Reference Field (*IGRF*) are updated every 5 years. The *IGRF* for the time and location of the survey is calculated and removed from the measured magnetometer value. Measurements recorded at a fixed location(s), *base station(s),* within the survey area are used to correct for the transient effects of the external field. Once the effect of the Earth's internal and external magnetic fields are removed from magnetometer readings, what remains is that portion of the magnetic field largely resulting from variations in the magnetic mineral content of near-surface rocks.

The most important minerals in geomagnetic studies are magnetite, pyrrhotite and titanomagnetite, as well as, oxides of iron, and oxides of iron and titanium (Telford et al., 1990). The overall magnetic response of a rock will, to a large extent, be determined by the proportion of these accessory minerals. Magnetic susceptibility (k) is the parameter that describes the capacity of a rock to be magnetized. Magnetite which has the largest magnetic susceptibility typically constitutes less than 2% of crustal minerals. Specific lithologies may exhibit a wide range of magnetic susceptibility although there appears to be a general trend of increasing magnetic susceptibility with decreasing quartz content. Rocks lose their magnetism at temperatures above ~580-630°C, corresponding to depths of ~20 - 40 km in continental regions with average geothermal gradients. In the survey areas, the geothermal gradient is high (~30°C/km, Hyndman and Lewis, 1999), and such temperatures are encountered at depths on the order of 20 km. Consequently, magnetic anomaly maps provide information on the distribution of magnetic (and non-magnetic) rocks only to this depth.

Magnetic responses within the Purcell Basin

Prior to the high-resolution survey described here, only low-resolution regional aeromagnetic data (flown at a mean terrain clearance of 300 m on flight lines spaced 800 m apart) were available for the survey areas. The results from the low-resolution regional survey governed expectations of the high-resolution data. It was expected that the increased resolution of the new data would provide significant enhancement of all anomalies visible in the regional data, and in addition, detect numerous small and/or low gradient anomalies not previously imaged. As outlined below, this indeed proved to be the case. Table 30-1 summarizes magnetic susceptibility measurements for more than 1000 rock samples from the survey areas. Measured values generally fall within published ranges (Telford et al., 1990). Sedimentary rocks are commonly non- to weakly-magnetic and, with the notable exception of the Creston Formation, those exposed within the survey areas have the typical low magnetic susceptibility values.

Moderate to intense magnetic anomalies (up to 340 nT) characterize portions of the middle Creston Formation (Fig. C20-4) where it is composed of green quartz arenite and arenaceous siltstone at upper greenschist metamorphism facies (Reesor, 1996). Hand specimens from magnetic green arenite contain abundant porphyroblastic magnetite (>2%). Lower and upper Creston Formation phyllite with little visible magnetite and middle Creston Formation maroon arenite containing hematite are, by comparison, poorly magnetized. Magnetic susceptibility measurements of the green quartz arenite unit, where it is proximal to large intrusions such as the White Creek batholith (Fig. C20-4a), are up to 20-30 times greater than arenite away from intrusions. However, magnetic susceptibilities of other units in the Creston Formation do not show this variation. This suggests that the magnetism of the green arenite is enhanced by contact metamorphism. The magnetic character of this unit (allowing the metamorphic stabilization of significant proportions of magnetite) suggests a unique chemistry relative to other units in the middle Creston Formation. The green arenite is also distinguished by relatively low radioelement concentrations (*see* Fig. C20-5a and discussion *below*). Even in regions where geological mapping of the middle Creston Formation is difficult because of overburden cover (for example, in the northern portion of the St. Mary River area) these geophysical properties allow it to be readily mapped. In western Montana, stratabound copper-silver deposits such as Troy, Montanore and Rock Creek are entirely restricted to the Revett Formation, which is correlated with the middle Creston Formation (Höy, 1993). The unique signatures of the middle Creston Formation therefore make airborne geophysical surveys a valuable tool for mapping the favourable stratigraphic interval for Cu-Ag deposits.

The lower Creston Formation typically comprises fine-grained argillite that commonly contains disseminated and stringer magnetite in the Yahk map area. This apparent restriction of magnetite in the lower Creston Formation to this part of the basin probably reflects original sedimentation conditions. It also results in the lower Creston Formation being unusually magnetic here and observed anomaly values are as high as those mapped in regions underlain by the middle Creston Formation elsewhere in the basin (typically 50 - 250 nT, Fig. C20-4a, b, c).

Pyrrhotite is pervasive throughout the Lower and Middle Aldridge Formation, and consequently it was expected that those units would display higher magnetic anomaly values than younger sedimentary units having significantly less pyrrhotite. However, this is not the case and consequently we infer that much of the pyrrhotite in the Lower and Middle Aldridge Formation must be monoclinic pyrrhotite in contrast to the Sullivan ore body where both monoclinic and magnetic hexagonal pyrrhotite are abundant (Ethier et al., 1976).

The average magnetic susceptibility value for gabbro is more than seventy times that of average sedimentary rocks (Telford et al., 1990). Measured values for gabbroic Moyie sills from within the survey areas (Table 20- 1), are at the low end of the published range of magnetic susceptibilities (average = 6.67×10^{-3} SI) but nonetheless more than six times higher than average values of the Lower and Middle Aldridge formation which they intrude. Consequently, it was expected that shallow and outcropping sills would be readily imaged and that magnetic anomaly data might provide a means of correlating sill outcrops along strike in regions of surficial cover. The sills were poorly imaged in existing regional aeromagnetic data due to the small outcrop area of the sills and the large line spacing of those surveys.

Table 20-1. Magnetic susceptibility and radioelement concentrations for selected geological units of the Purcell anticlinorium as determined by ground measurements in the field, or by laboratory measurement on hand and core samples. Units shown in italics are alteration or textural types associated with Sedex mineralization in the Lower and Middle Aldridge.

Age	Geological Unit	Magnetic Susceptibility			Mean Radioelement Concentration						
		(10^{-3}SI)			K %		eU (ppm)		eTh (pm)		
		Mean	Range	No. of Measurements	Mean	Range	Mean	Range	Mean	Range	No. of Measurements
Mesozoic	Intrusive rocks	6.53	0-33.9	150	4.51	2.9-6.12	6.34	4.58-8.1	16.51	14.1-18.92	2
	Reade Lake stock	7.09	0.3-24	80	4.94	4.7-5.2	7.28	5.2-8.3	16.50	13-22.6	5
	White Creek batholith	12.36	5- 35.7	40							
	America Creek stock	0.30	0-1.26	20	2.90		4.40		14.10		1
	Angus Creek stock	7.00	4.2-12.9	10							
	Hall Lake stock	3.15	0-7.5	20							
Paleozoic	Cranbrook Formation	0.27	0-54	70	2.1	0.1-3.2	3.39	2.2-4.7	11.72	1-19.6	7
	Eager Creek Formation	1.40	0-2.51	20							
Upper Proterozoic	Horsethief Creek Formation	0.87	0-1.3	30	2.15	1.6-2.7	1.3	1.2-1.4	5.6	5.3-5.9	2
	Toby Formation	0.69	0.4-1.14	15							
Middle Proterozoic	Hellroaring Creek stock	0.16	0.02-0.5	50	4.22	2.8-6.3	3.78	1.4-7.3	2.72	1.3-3.7	5
	Moyie sills	6.67	0-160	200	1.11	0.7-2.2	1.31	0.2-2.3	4.59	2.2-9.0	8
	Creston Formation	15.2	0-125.7	330	2.10	1.9-5.2	2.90	1.8-4.7	11.24	9.2-21.6	7
	Upper Aldridge Formation	0.42	0-2.5	40	3.20	2.8-3.6	3.00	2.8-3.2	17.30	15.7-18.9	2
	Middle Aldridge Formation	0.72	0-40.2	120	3.51	1.8-5.4	3.61	2.4-4.7	12.90	9.3-21.6	1
	Lower Aldridge Formation	0.67	0-5	350	3.27	1.1-6.2	3.79	1.2-5.5	12.24	7.4-23.4	9
	sedimentary fragmental	*0.63*	0-2	80	*3.67*	3-4.2	*5.08*	4.4-5.6	*17.23*	16-20.9	8
	garnet-bearing	*7.30*	0.04-40.2	20	*3.25*	2.9-3.7	*6.55*	4.2-9.1	*12.00*	8.7-16.1	7
	muscovite-, sericite bearing	*0.78*	0-2.36	35	*3.74*	2.8-4.43	*3.85*	2.6-5.1	*16.9*	9.8-19.9	9
	albite-bearing	*0.20*	0-0.45	10	*4.00*	3.75-4.25	*3.20*	2.6-3.8	*19.00*	16.9-22	2
	tourmaline-bearing	*0.16*	0.11-0.3	20	*2.75*	0.2-4.2	*4.02*	3.2-4.3	*15.53*	13.5-17.2	5

Analysis of the high-resolution data complemented by ground follow-up investigations led to new identifications of several sill exposures and even in regions of thick glacial cover, such as north of the St. Mary River, the data allowed sills to be correlated along strike. An arch of gabbroic sill is a feature of the Sullivan - North Star corridor (Turner et al., 2000a) and their recognition elsewhere may be important for mineral exploration. In all regions the magnetic response of Moyie sills is quite variable; the majority are poorly magnetized and in many instances an anomaly is observed only over a portion of a sill outcrop. Magnetic sills show a clear association with mapped faults, or are proximal to large intrusions indicating a secondary thermal or possibly hydrothermal origin for the magnetism. This is especially clear for the package of sills outcropping immediately south of the White Creek batholith in the St. Mary area (Fig. C20-4a). Sill segments within the aureole of the intrusion yield significantly higher magnetic anomaly and magnetic susceptibility values than those farther away. Similarly, follow-up ground studies identified gabbro as the source of several small magnetic anomalies proximal to the Hall Lake and St. Mary fault systems (Fig. C20-4a), as well as the string of anomalies extending west-southwest from the Emily Creek Fault in the Findlay area (Fig. C20-4b). The package of Moyie sills exposed in the Hawkins Creek area to the east of the Yahk fault is geophysically atypical, corresponding with higher than average magnetic anomaly values (Fig. C20-4c), moderate apparent conductivities (Fig. C20-3a; up to 10 ms/m; 100 ohm-m on the 56000 Hz coil pair) and elevated K values (not shown here).

Igneous rocks commonly display a wide range of magnetic susceptibility values (Telford et al., 1990). S-type granites, which form by anatexis of metasedimentary rocks, typically are preferentially enriched in ilmenite and tend to have low magnetic susceptibility values. In contrast, I-type granites having a mafic-rich source typically are preferentially enriched in magnetite, and consequently tend to have high magnetic susceptibility values. However, assimilation, metasomatic and/or metamorphic processes, during or subsequent to the emplacement of magma, can alter the chemistry and mineralogy of parts or the whole of an intrusion. Although some workers have suggested that Jurassic intrusions within the Purcell basin may have an I-type affinity (Brandon and Lambert, 1993), little has been published on the affinity of these or the younger Cretaceous bodies. Magmatic differentiation within a large intrusion can lead to spatial variations in magnetic mineral content (magnetite is often preferentially enriched in early mafic phases relative to younger felsic phases). Consequently, it was expected that magnetic anomaly values over small undifferentiated bodies such as the Hall Lake and Sawyer Creek plutons (Fig. C20-4a) would be more uniform than those over the differentiated White Creek and Fry Creek batholiths.

Two magnetically distinctive suites of Cretaceous intrusions were recognized within the survey areas. The White Creek batholith has a weakly magnetic central region and a strongly magnetic margin (Fig. C20-4a, b). This characteristic is also visible in regional magnetic anomaly data (Cook et al., 1995). The magnetic margin is heterogeneous and discontinuous; peak margin amplitudes vary from ~140 nT to >850 nT and the width varies from <500 m to >3 km. High intensity marginal phases correlate with the distribution of biotite monzogranite and hornblende granodiorite phases (units Kwc3 and Kwc2; Reesor, 1996) and lower intensity interior phases with biotite-muscovite leuco monzogranite (unit Kwc4, Reesor, 1996). Contrary to expectation, the Hall Lake pluton and Sawyer Creek stock display similar magnetic characteristics. However, in the case of the Hall Lake stock the magnetic margin is only observed over the northern portion of the body and in the case of the Sawyer Creek stock, only over the southern portion of the stock. Hornfelsed host rocks adjacent to the intrusions are common. The measured magnetic susceptibility of hornfels containing porphyroblastic magnetite ± pyrrhotite is significantly elevated compared to unaltered host rock indicating secondary magnetization of the country rocks.

In contrast, older regional, as well as the new high-resolution magnetic data show that the Fry Creek batholith and the Reade Lake stock (exposed a few kilometres east of St. Mary River area) are characterized by high magnetic values throughout their mapped exposures reflecting a more homogeneous distribution of magnetic minerals in these bodies. (Note: although the Reade Lake Stock does not outcrop within the St. Mary Survey area, the magnetic anomaly associated with it extends into the survey area; Fig. C20-4a). Petrographic studies of the Reade Lake stock by Höy (1993) identified disseminated magnetite. Exposures of this stock are limited and its mapped contact was drawn from regional magnetic anomaly data (Höy and van der Heyden, 1988). Ground follow-up studies showed that outcrops of Eager Creek Formation siltstone occur in areas previously mapped as Reade Lake stock. The siltstone and nearby exposures of Creston Formation adjacent to the stock have elevated magnetic susceptibilities compared with the measured averages of these formations (Table 20-1), which suggests a secondary magnetization. Thus, the stock is not as extensive as previously inferred. Radioelement patterns over the Cretaceous intrusions generally complement magnetic data in that they are elevated in non- to weakly-magnetic felsic rocks and relatively low in more magnetic, mafic units. Together these two methods offer a means of remotely recognizing subtle lithologic changes within intrusions where detailed field mapping is lacking. A spatial association between Cretaceous intrusions, lode gold mineralization and placer deposits highlights the possible applications of combining magnetic and radiometric data in the exploration for these deposit types by identifying specific types of intrusions or deposit trains from them.

Faults can have a variety of expressions on magnetic anomaly maps. If the fault juxtaposes units with contrasting magnetic susceptibilities it will generate a magnetic lineament parallel to the fault trend, and a steep magnetic gradient perpendicular to the fault trend. Faults, which juxtapose units with comparable magnetic susceptibility values, will be magnetically invisible. Movement of fluids along fault zones may produce zones of hydrothermal mineralization and alteration containing magnetic minerals that may then result in prominent magnetic lineations.

Most of the mapped faults within the survey areas offset weakly magnetic sedimentary rocks against weakly magnet-

ic sedimentary rocks and, with the exception of a number of faults in the Yahk area, were not directly imaged in the magnetic anomaly data. However, as discussed above, highly magnetic segments of Moyie sills adjacent to faults form strings parallel to the traces of several faults and provide indirect evidence for the faults. Such is the case along the St. Mary Fault (Fig. C20-4a). Mapped and inferred faults that cut similar stratigraphy in the Yahk survey area (Fig. C20-4c), e.g. the Iron Range, Spider and Moyie faults, are associated with linear zones of moderate to steep magnetic gradient (maximum gradients of approximately 0.21, 0.12 and 0.16 nT/m, respectively). Magnetic sources in the latter cases are magnetite-hematite breccias (Stinson and Brown, 1995).

The north-trending Iron Range fault zone is the most spectacularly imaged fault within the survey areas (Fig. C20-4c) producing an intense linear magnetic anomaly with a peak amplitude of 1130 nT. The width of this anomaly varies from less than 1 km to about 4 km. Ground follow-up studies confirm that the primary magnetic sources are the 0.3 - 5 m wide massive lenses of magnetite and hematite which grade outward to wider, less-brecciated, magnetite-rich zones. Original magnetite abundances in these lenses and breccias range from 5 to 30%, but most is now pseudomorphed by hematite (Stinson and Brown, 1995). The highest magnetic susceptibility values in the entire survey were measured in these massive lenses (> 400 x 10^{-3} SI). Peaks in magnetic intensity along the fault zones where no magnetite-rich lenses are mapped may be indicative of buried lenses, although elevated anomaly values are also associated with disseminated magnetite and altered Moyie sills in and adjacent to fault zones. The Iron Range fault is also well imaged radiometrically (Fig. C20-5c).

Contrary to expectation, exposures of Nicol Creek basaltic lava in the St. Mary River area could not be distinguished magnetically, although outside the survey areas these lavas may be mapped by their intense magnetic anomalies. Original geochemical differences or subsequent metamorphic overprints are possible explanations of the observed difference.

Gamma-ray spectrometry

Principles and methodology

Gamma-ray spectrometry is a geophysical technique that provides geochemical information on the top few tens of centimetres of the Earth's surface. As with any near-surface geochemical method, interpretation requires an understanding of the nature of the surficial materials, such as tills, glacial outwash, fluvial, or lacustrine deposits and their relationship to bedrock.

Potassium (K), uranium (U), and thorium (Th) are major, mobile trace, and immobile trace elements, respectively. They are present in variable amounts in all rocks and derived materials. Radioelement signatures of minerals, as measured from the gamma-ray spectrometric survey, assist in lithological mapping. K concentrations are measured directly from the airborne gamma-ray spectra, whereas U and Th concentrations are computed from the spectra of their daughter products, Bi^{214} and Ti^{208}, respectively, which are more readily distinguished from the other gamma rays in the spectrum. Where the "normal" distribution of these elements (K, eU – equivalent uranium, eTh - equivalent thorium) is disrupted by a mineralizing process the resultant radioelement anomaly provides direct exploration guidance.

In general, radioelement data complement magnetic data, as radioelement values tend to be elevated in non- to weakly-magnetic, evolved felsic and sedimentary rocks and relatively low in less evolved, more magnetic, mafic units. A more thorough summary of gamma-ray spectrometry theory, techniques, and Canadian case histories is presented in Shives et al. (1995).

For the current surveys, the gamma-ray spectrometric system consisted of a 16 L sodium iodide crystal array attached to a 256 channel Exploranium GR820 spectrometer. A 4 L upward looking crystal was used to monitor background radiation.

Gamma-ray responses within the Purcell Basin

Addition of gamma-ray spectroscopy to the more conventional EM-magnetic surveys was expected to provide important new geochemical information not previously gathered within the Purcell basin. Although airborne and ground gamma-ray spectrometry have been successfully applied to geological mapping and exploration for a variety of mineral deposit types worldwide, the current surveys provide the first Canadian test over a geological terrain containing Sedex deposits. By using the measured radioelement concentrations as a guide to geochemical variations it was anticipated that the large intrusions, and possibly phases within them, could be delineated, and, also that subtle facies or formational variations within the Purcell Supergroup stratigraphy could be differentiated. Of particular interest was whether the muscovite alteration that envelopes the Sullivan deposit and occurs extensively in the Sullivan - North Star corridor (Turner et al., 2000b) could be distinguished from the regionally metamorphosed biotite- and muscovite-bearing sedimentary rocks of the Purcell basin.

Within the three areas surveyed, rugged topography and variable bedrock exposure significantly influence the total radioactivity measured. South-facing slopes are relatively drier, less vegetated, and have more exposed bedrock and talus than north-facing slopes. Consequently, south-facing slopes yield higher radioelement concentrations that are more representative of bedrock values. This is especially obvious in measured K concentrations (*see* K map in British Columbia Ministry of Employment and Investment, 1996). These effects were minimized by using radioelement ratios (eU/eTh, eU/K, and eTh/K) to distinguish important relative variations among the three elements. Air photographs and landsat images, which allowed regions of exposed bedrock to be readily distinguished from regions of dense vegetation and/or surficial cover, were also useful aids in the interpretation of radioelement data.

Regionally, a number of distinct radioelement anomalies and patterns were recognized (Fig. C20-5). Very low eTh/K ratios delineate the distinctive chemistry of the Proterozoic Hellroaring Creek (Fig. C20-5a) and Greenland Creek stocks (Fig. C20-5b). These highly evolved intrusions contain aplitic and pegmatitic phases comprised of quartz, mus-

covite, sodic plagioclase, microcline feldspar, and minor garnet, beryl, tourmaline, and pyrite. In addition, radioelement variations within the White Creek batholith correlate with mapped phases (Reesor, 1996) and clearly distinguish this batholith from the smaller Sawyer Creek and Hall Lake stocks of Cretaceous age within the St. Mary River area which are characterized by lower radioelement concentrations (Fig. C20-5a).

Outcropping Moyie sills were recognized by low radioelement concentrations (approximately one third lower than the Lower or Middle Aldridge Formation, Table 20-1). Together with magnetic anomaly data this correlation offers assistance for improved sill delineation. An exception to this general rule is the sill package that crops out east of the Yahk Fault and north of Hawkins Creek. Not only is this package characterized by moderate K concentrations (*see* K map in British Columbia, Ministry of Employment and Investment, 1996), but as discussed above it is also electromagnetically and magnetically anomalous.

Along the southern and western edge of the St. Mary survey area, high eTh/K ratios accurately demarcate a quartzite member within the Horsethief Creek Group (Fig. C20-5a, unit HH_2 of Reesor, 1996). The radiometric anomaly is caused by extremely low K contents and elevated thorium-bearing accessory minerals in the quartzite. Farther to the northwest, EM data delineate agillaceous units within this same formation (*see* discussion *above*). West of the Carroll Fault in the Yahk area, high K concentrations (not shown here) correspond with zones of enhanced conductivity associated with graphitic mudstones and carbonaceous argillites in the Middle and Upper Aldridge Formation.

Immediately east of the Hall Lake fault near the southern boundary of the Saint Mary survey area broad areas of elevated eU and eTh values correlate with argillaceous units in the Upper Aldridge and lower Creston formations. Reesors's (1996) mapping of these units in this area supports this correlation, suggesting that extension of the contacts of these units into unmapped areas is possible using airborne radioelement patterns. The lower/middle Creston boundary is recognized by a decrease in eU and eTh levels (and a corresponding increase in eTh/K ratios, Fig. C20-5a), and as described above, is coincident with the transition from low to moderate magnetic anomaly values. These strong and complementary radioelement/magnetic relationships highlight the advantages of multi-technique geophysical surveys and integrative interpretation.

Many examples of fault-controlled iron-oxide mineralization and albite-sericite alteration occur within the survey areas. A belt of elevated eTh/K values along the Iron Range fault zone (Fig. C20-5c) correlates with albite-rich breccias in the fault zone, regions of extensive albitic alteration adjacent to the fault zone, and apophyses of albite-rich material that extend up to a few metres into adjacent Moyie sills (Stinson and Brown, 1995). The most intense anomalies correspond to areas where albite alteration is most intense as at Iron Range Mountain, Mount Thompson, and west of the Sha occurrence (Fig. C20-5c).

Absorption of gamma rays in water results in depleted radioelement concentrations along all of the major drainages and lakes (*see* K map in British Columbia Ministry of Employment and Investment, 1996). However, unconsolidated deposits in these drainages, such as the St. Mary River, Redding Creek, Goat River, Hawkins Creek and Kitchener Creek typically yield elevated eTh/K ratio patterns. These patterns are interpreted as reflecting elevated levels of stable thorium bearing minerals associated with heavy mineral concentrations in the valley floors.

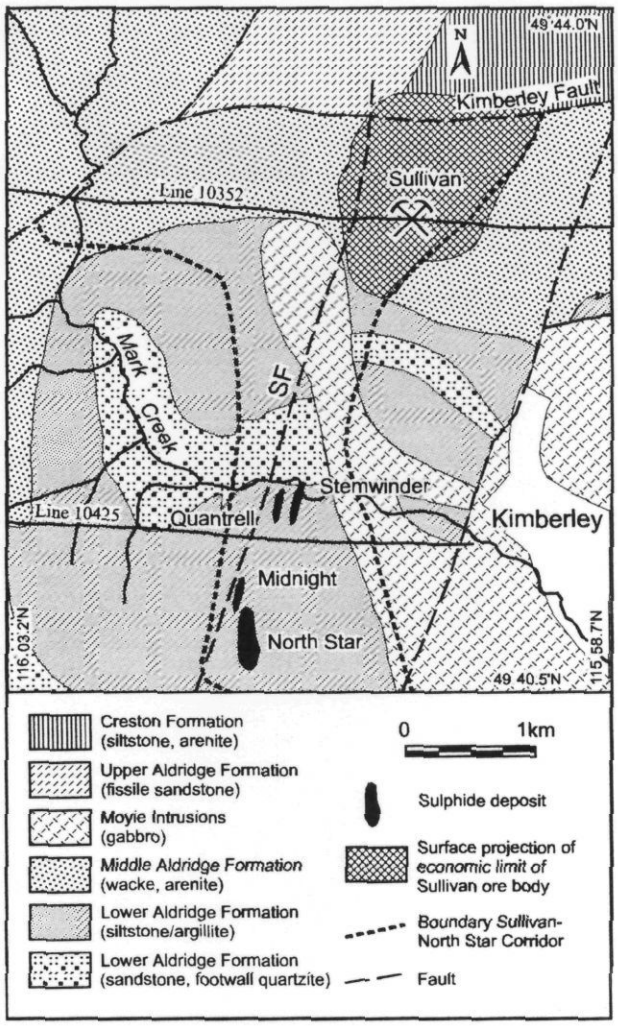

Figure 20-6a. Geological map of the Sullivan-North Star corridor (modified from Hagen (1985) and Turner et al., (2000a)). The boundary to the Sullivan Corridor marks the extent of pervasive, pre-gabbro, hydrothermal alteration and sulphide mineralization.

VLF

The marine transmitter station operated only discontinuously during the survey. In addition, VLF data had a low signal-to-noise ratio, due in part to the resistive nature of the geological units encountered. Although these data may contain some information useful for identifying and/or refining conductors in the near surface they are generally of poor quality and are not considered here.

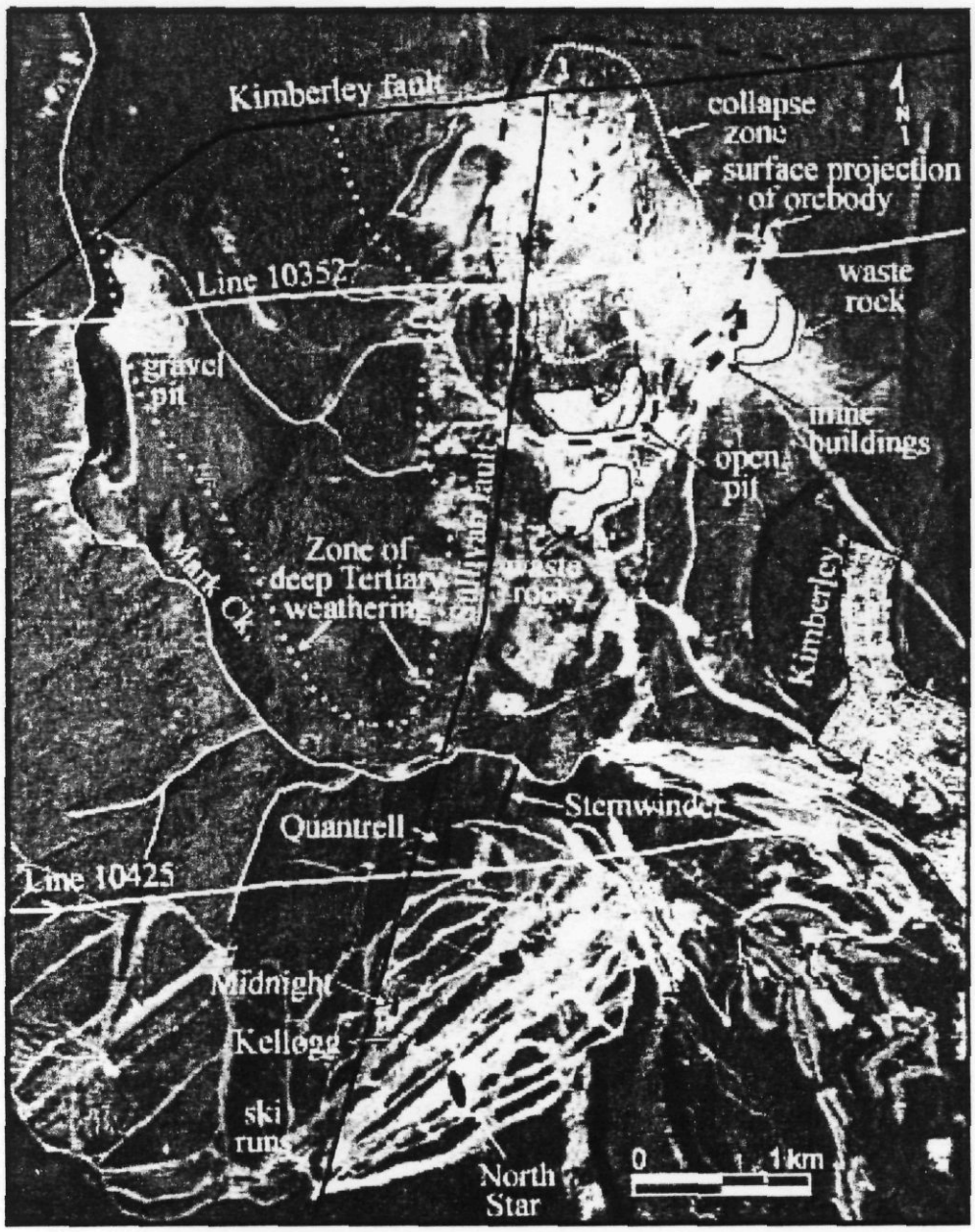

Figure 20-6b. Surface features in the Sullivan-North Star corridor. Airphotograph supplied by Cominco Ltd. (photo FFC94016-19, August 10, 1994). Arrows on flight lines indicate direction of helicopter during data acquisition. The extent of the deep Tertiary weathering zone is taken from P. Ransom (unpub. data, 1996).

THE SULLIVAN - NORTH STAR CORRIDOR

To assess the utility of the three geophysical techniques for mineral exploration we next examine the observed responses within the Sullivan - North Star corridor where a number of significant deposits occur (Fig. 20-6). As discussed above, the quantity and connectivity of sulphide minerals in a mineralized zone will, to a significant extent, determine its overall conductivity. Both pyrrhotite and to a much lesser extent, magnetite (average magnetic susceptibility = 1.5, 6 SI, respectively, Telford et al., 1990) are associated with sulphide mineralization in the Purcell Basin and significant muscovite, albite and/or chlorite alteration of the host rocks is typical in many cases. Consequently, it was expected that mineral occurrences within the corridor would correspond with zones of enhanced conductivity, strong finite conductors, high magnetic anomaly values and low eTh/K anomalies. Despite nearly complete extraction of ore from the Sullivan mine, it gives a significant EM and magnetic response. Also, altered and barren- to weakly- mineralized waste rock on the surface around the deposit corresponds with subtle to intense magnetic, EM, and radioelement anomalies (Fig. 20-6 and C20-7).

Strong finite conductors, that cannot be attributed to cultural features, are coincident with the surface projection of the sulphide-rich Sullivan horizon, especially along the west side of the deposit where it is cut by the Sullivan fault, and along the south side of the open pit (Fig. 20-6 and C20-7a). The Sullivan fault zone contains pyrrhotite at depth and this pyrrhotite is a likely cause for some conductors. The conductors are typically quite broad, with in-phase and quadra-

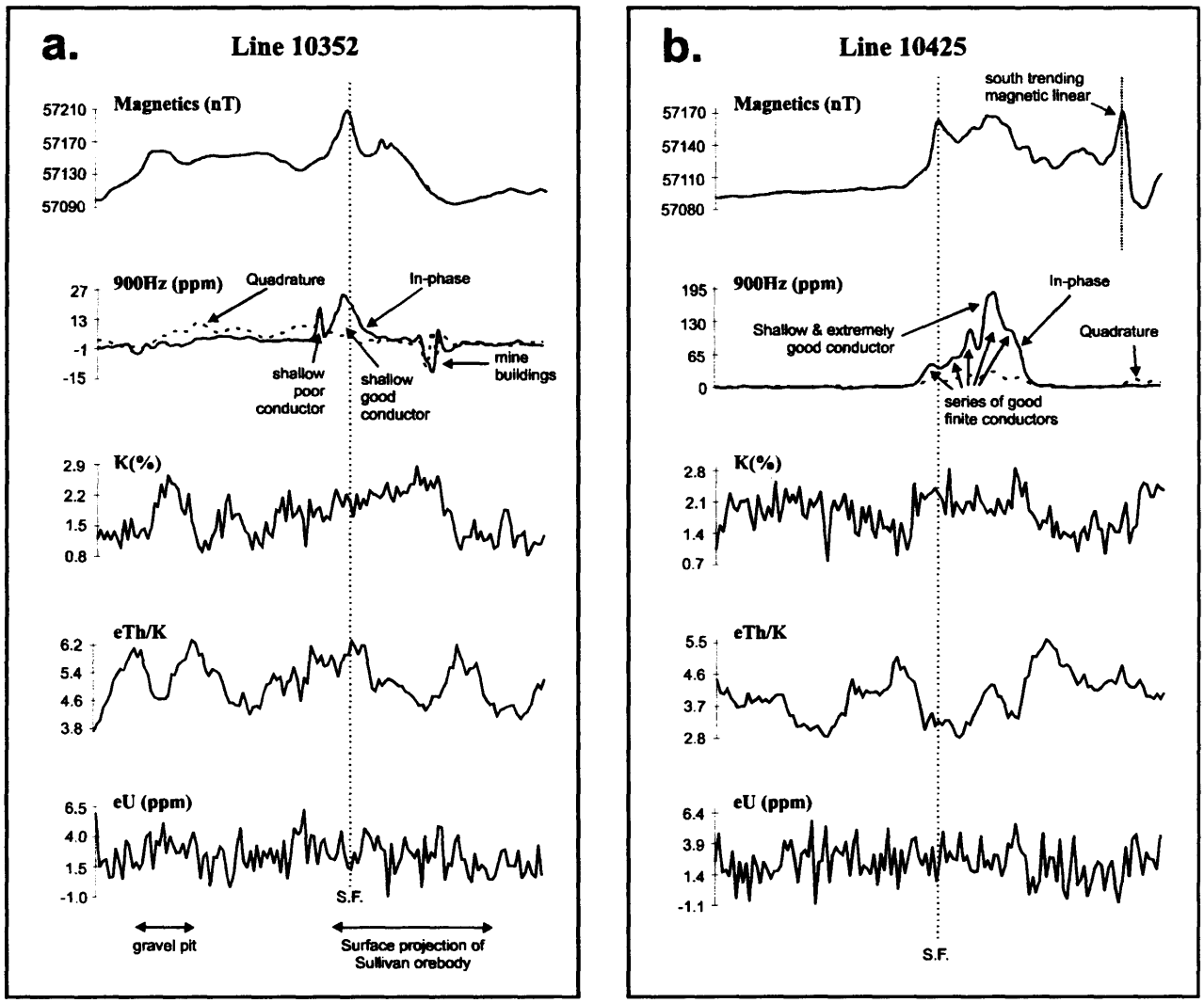

Figure 20-8. Stacked profiles of eU, eTh/K, K, conductivity (900 Hz coaxial data) and magnetic anomaly values along flight lines: **(a)** 10352, over the Sullivan mine; and **(b)** 10425, just south of the Stemwinder deposit. SF = Sullivan fault. See Figure C20-7 for location of flight lines.

ture values, which are generally larger than 15 ppm (Fig. C20-7 and 20-8). The conductors have large conductance values, as calculated from the 900 Hz coaxial data, assuming a two-dimensional vertical conductor in free space. In general, the deeper a conductor is buried the lower the absolute values of both the in-phase and quadrature components. However, the ratio of the in-phase and quadrature components is only slightly affected by burial depth, so it is an important indicator of absolute conductivity. Conductors related to cultural features include mine buildings, heavy equipment, and power lines.

Enhanced conductivity is attributed to the undisturbed massive pyrrhotite body (up to 50 m thick and 500 m long) that underlies the ore zone in the western and shallowest part of the underground workings, and to unmined massive sulphide ore. The collapse zone, which overlies the most extensively mined zone, is not anomalous.

The most prominent cluster of finite conductors within all three, survey areas occurs over an area 1.0 km by 1.2 km in the vicinity of the North Star and Stemwinder mines. It comprises shallow conductors with greater conductance values than those at Sullivan (Fig. 20-8). The conductors are attributed to north-trending sulphide-rich zones, including veins of the abandoned workings and zones consisting of abundant sulphide-filled fractures. An associated zone of enhanced conductivity terminates where the Stemwinder vein pinches out north of Mark Creek, in an area of thick cover and deep weathering (compare Fig. 20-6b and C20-7a). This deep weathering zone comprises oxidized and friable bedrock up to 146 m deep.

A moderately positive, irregularly-shaped (4.5 km by 3.2 km) magnetic anomaly is observed in the corridor area (Fig. C20-7b). Localized zones of elevated anomaly values occur over the Sullivan mine, between the North Star and Stemwinder deposits and over exposures of Moyie sill. The magnetic anomaly is truncated to the north by the north-dipping Kimberley fault. The western and southern boundaries are less well defined. To the east, the anomaly abruptly ter-

minates at a narrow (< 500 m wide), south-trending magnetic linear that extends from the St. Mary River valley to the Kimberley fault (Fig. C20-4).

Zones of enhanced magnetic anomaly values at the Sullivan mine correspond to the shallowest portions of the mineralized zones adjacent to the Sullivan fault (Fig. C20-7b, 20-8). The magnetic peak at Sullivan is primarily due to the massive pyrrhotite replacement body beneath the western portion of the ore body. Most of this pyrrhotite must only be weakly magnetic, otherwise a stronger anomaly would be expected. Although the eastern portion of the ore body contains minor magnetite (Hamilton et al., 1982) its concentration does not appear to be high enough to affect magnetic amplitudes. The magnetic peak at North Star is situated between the North Star and Stemwinder mines, where abundant disseminated and fracture-filled pyrrhotite occurs. As at the Sullivan Mine, the magnitude of the anomaly suggests that a considerable proportion of the pyrrhotite must be weakly magnetic. North of the Stemwinder Mine lower magnetic amplitudes correspond to the zone of thick Quaternary cover and deep bedrock weathering (*see* Fig. 20-6b).

Elevated radioelement (K, eU, and eTh) concentrations are associated with the Sullivan open pit, collapse zone and waste dumps (Fig. C20-7c, d and 20-8). These anomalies are enhanced by increased bedrock exposure and drainage relative to the surrounding undisturbed, vegetated, moist overburden. Ground spectrometry confirmed the elevated concentrations. Subtle depressed eTh/K ratios are apparent over the eastern and southern waste dumps, but not over the open pit or collapse area. This suggests that the mine waste rock contains more K than does surface bedrock and surficial materials. The area of elevated K, eU and eTh values extends northward from the pit area, across the Kimberley fault and over exposures of the Upper Aldridge Formation on Sullivan Hill. North of the Kimberley fault the radioelement patterns reflect their abundances in the Upper Aldridge argillite and are not related to the mineralization and alteration that characterize the Sullivan-North Star corridor.

Elevated radioelement concentrations and low eTh/K ratios also occur over the North Star deposit. In situ spectrometry on bedrock and talus confirms K enrichment relative to unaltered Aldridge turbiditic sediments. The enrichment is a result of sericite alteration within a narrow sub-vertical zone that extends 2 km to the south. These patterns are enhanced by increased bedrock exposures related to old mine workings, cleared ski runs or talus.

Lower amplitude K enrichments with coincident eTh/K depletions occur west and northwest of North Star Hill, in steeply sloping or bowl-shaped areas covered with very thick clay-rich till. Although these anomalies accurately reflect the relatively K-rich chemistry of the till, the corresponding low magnetic anomaly values suggest that the radioelement anomalies do not represent exploration targets like those known within the Sullivan-North Star corridor.

Associated with the mineralization in this corridor are growth faults, chaotic breccia, Moyie sills, manganiferous garnet-rich beds and muscovite and albite-biotite-chlorite alteration (Turner et al., 2000b). The rock property measurements (Table 20-1) show that relative to most Aldridge sedimentary rocks, sedimentary fragmentals have moderately higher K and eU concentrations, those rich in garnet porphyroblasts have higher magnetic susceptibilities and higher eU concentrations and those that exhibit muscovitic and sericitic alteration have elevated K concentrations and relatively lower eTh/K ratios. Although tourmaline-bearing Aldridge rocks appear to have lower magnetic susceptibility values and to be moderately enriched in eU and eTh relative to unaltered Aldridge sedimentary rocks few samples were available for analysis. More extensive chemical analyses of tourmalinites (Jiang et al, 2000a, b; Slack et al., 2000) do not support relative radioelement enrichment in these rocks.

SUMMARY

The new geophysical data described here permit a refinement of geological interpretations and maps within the survey areas. The shallow sampling depths of the gamma-ray spectrometric and EM methods make them particularly suitable for mapping the surface extent of units whose geophysical signatures contrast with adjacent units. Several new exposures of Moyie sills have been identified using the data, and it has proved possible to correlate sills along strike using their characteristic high apparent resistivities (generally > 5000 ohm-m; <0.2 mS/m), low radioelement concentrations and elevated magnetic anomaly values compared to adjacent sedimentary rocks (Table 20-1). Similarly, radioelement data allow the surface extent of the Proterozoic Hellroaring Creek and Greenland Creek stocks to be mapped more accurately. Zones of low apparent conductivity in the St. Mary area accurately outline exposures of the quartzites in the Horsethief Creek Group (unit HH_2 of Reesor, 1996) formations. Extremely low K content and elevated thorium-bearing accessory minerals in unit HH_2 result in high eTh/K ratios.

The new geophysical data for the Sullivan - North Star corridor provide baseline information for mineral exploration elsewhere in the Purcell Basin. Elevated magnetic values, high electrical conductance, and low eTh/K ratios are characteristic of mineralization and sericitic alteration in the corridor, even in the vicinity of the Sullivan deposit where about 90% of the ore has been removed. Outside of the corridor, the Aldridge Formation typically is characterized by low magnetic values, low electrical conductivities, and by relatively few and relatively weak finite bedrock conductors. This suggests that undiscovered magnetic massive sulphide accumulations in the survey areas must be more deeply buried than the near surface portions of either the Sullivan or the North Star deposits. However, it does not preclude the presence of disseminated sulphides at any depth.

ACKNOWLEDGEMENTS

This manuscript has benefited from thorough critical reviews by J.W. Lydon, K. Ford, J.F. Slack, and an anonymous reviewer. We thank D. Anderson, S. Coombes, T. Höy, C. Kennedy, P. Klewchuk, P. Ransom, T. Termuende, B. Turner and B. Woodfill for freely sharing their geological expertise of the area. In addition, B. Woodfill supplied numerous samples for the physical property measurements. R. Franklin, V. Vilkos and J.W. Lydon prepared the figures.

REFERENCES

Anderson, D.
1985: Diamond drilling report, Vulcan Property; B.C. Energy, Mines and Petroleum Resources, Assessment Report 14,198, 21p.

Anderson, H.E. and Davis, D.W.
1995: U-Pb geochronology of the Moyie sills, Purcell Supergroup, southeastern British Columbia: implications for the geological history of the Purcell (Belt) basin; Canadian Journal of Earth Sciences, v.32, p.1180-1193.

Brandon, A. D. and Lambert, R. StJ.
1993: Geochemical characterization of mid-Cretaceous granitoids of the Kootenay Arc in the southern Canadian Cordillera; Canadian Journal of Earth Sciences, v.30, p.1076-1090.

British Columbia Ministry of Employment and Investment
1996: East Kootenay Geophysical Survey, Open File 1996-23 (eighteen 1:50 000 scale geophysical images).

Brown, D.A., Bradford, J.A., Melville, D.M., and Stinson, P.
1995: Geology and Mineral Occurrences of the Yahk map area, southeastern British Columbia (82F/1); British Columbia Ministry of Energy, Mines and Petroleum Resources, Open File 1995-14, scale 1:50 000.

Brown, D. A., Lowe, C., Shives, R.B.K., and Best, M.E.
1997: The East Kootenay geophysical survey, southeastern British Columbia (82F, G, K) - Sullivan - North Star Area; in Geological Fieldwork 1996, (ed.) D.V. Lefebure, W.J. McMillan, and J.G. McArthur; British Columbia Geological Division, Paper 1997-1, p.3-15.

Cook, F.A., Varsek, J., and Thurston, J.B.
1995: Tectonic significance of gravity and magnetic variations along the Lithoprobe Southern Canadian Cordillera Transect; Canadian Journal of Earth Sciences, v.32, p.1584-1610.

Ethier, V.G., Campbell, F.A., Both, R.A., and Krouse, R.A.
1976: Geological setting of the Sullivan orebody and estimates of temperatures and pressures of metamorphism; Economic Geology, v.71, p.1570-1588.

Fraser, D.C.
1975: Resistivity mapping with an airborne EM system; Geophysics, v.43, p.144-172.

Hagen, A.S.
1985: Sullivan - North Star Corridor; Unpublished report, Cominco Ltd., 11p.

Hamilton, J.M., Bishop, D.T., Morris, H.C., and Owens, O.E.
1982: Geology of the Sullivan Ore body, Kimberley, B.C., Canada; in Precambrian sulphide deposits, (ed.) R.W. Hutchinson, C.D. Spence, and J.M. Franklin; Geological Association of Canada, Special Paper 25, H.S. Robinson Memorial Volume, p.597-665.

Höy, T.
1984a: Structural setting, mineral deposits, and associated alteration and magmatism, Sullivan camp, southeastern British Columbia; in Geological Fieldwork 1983; British Columbia Ministry of Energy, Mines and Petroleum Resources, Paper 1984-1, p.24-35.

1984b: Geology of the Cranbrook sheet and Sullivan map area; British Columbia Ministry of Energy, Mines and Petroleum Resources, Preliminary Map 54, scale 1:50 000.

1993: Geology of the Purcell Supergroup in the Fernie west-half map area, southeastern British Columbia; British Columbia Ministry of Energy, Mines and Petroleum Resources, Bulletin 84, 157p.

Höy, T. and van der Heyden, P.
1988: Geochemistry, geochronology, and tectonic implications of two quartz monzonite intrusions, Purcell Mountains, southeastern British Columbia; Canadian Journal of Earth Sciences, v.25, p.106-115.

Höy, T., Anderson, D., Turner, R.J.W., and Leitch, C.H.B.
2000: Tectonic, magmatic and metallogenic history of the early syn-rift phase of the Purcell basin, southeastern British Columbia; in The Geological Environment of the Sullivan Deposit, British Columbia, (ed.) J.W. Lydon, J.F. Slack, T. Höy, and M.E. Knapp; Geological Association of Canada, Mineral Deposits Division, MDD Special Volume No. 1, p.

Höy, T., Price, R.A., Legun, A., Grant, B., and Brown, D.A.
1995: Purcell Supergroup, southeastern British Columbia, compilation map; British Columbia Ministry of Energy, Mines and Petroleum Resources, Geoscience Map 1995-1, scale 1:250 000.

Hyndman, R.D. and Lewis, T.J.
1999: Geophysical consequences of the Cordillera-Craton thermal transition in southwestern Canada; Tectonophysics, v.306, p.397-422.

Jiang, S.-Y., Palmer, M.R., Slack, J.F., and Anderson, D.
2000a: Chemical and Boron Isotopic Composition of Tourmaline from Massive Sulphide Deposits and Tourmalinites in the Mesoproterozoic Belt and Purcell Supergroups, southeastern British Columbia and northwestern Montana; in The Geological Environment of the Sullivan Deposit, British Columbia, (ed.) J.W. Lydon, J.F. Slack, T. Höy, and M.E. Knapp; Geological Association of Canada, Mineral Deposits Division, MDD Special Volume No. 1, p.

Jiang, S.-Y., Palmer, M.R., Slack, J.F., Yang, J.-H., Shaw, D.R.
2000b: Trace Element and Rare Earth Element Geochemistry of Tourmalinite and Related Rocks and Ores from the Sullivan Pb-Zn-Ag Deposit and Vicinity, southeastern British Columbia; in The Geological Environment of the Sullivan Deposit, British Columbia, (ed.) J.W. Lydon, J.F. Slack, T. Höy, and M.E. Knapp; Geological Association of Canada, Mineral Deposits Division, MDD Special Volume No. 1, p.

Keller, G.V. and Frischknect, F.C.
1966: Electrical methods in geophysical prospecting; Pergamon Press, Oxford, United Kingdom, 517p.

Leech, G.B.
1957: St. Mary Lake, Kootenay District, British Columbia (82F/9); Geological Survey of Canada, Preliminary Map 15-1957, scale 1:63,360.

Lowe, C., Brown, D.A., Best, M.E., and Shives, R.B.K.
1997: The East Kootenay Multiparameter Geophysical Survey, southeastern British Columbia - Regional synthesis; in Current Research, part A; Geological Survey of Canada, Paper 97-1A, p.167-176.

Lowe, C., Brown, D.A., Best, M.E., Woodfill, R., and Kennedy, C.
1998: New geophysical data from the Yahk map area, southeastern British Columbia - part of the East Kootenay multiparameter geophysical survey; in Current Research, 1998-A; Geological Survey of Canada, p.207-216.

Nabighian, M.N. (editor)
1987: Electromagnetic methods in applied geophysics – theory, Volume 1; Society of Exploration Geophysics, Tulsa, Oklahoma, 510p.

Palacky G.J.
1987: Resistivity characteristics of geologic targets; in Electromagnetic methods in applied geophysics - Theory, (ed.) M.N. Nabighian; Society of Exploration Geophysicists, Tulsa, Oklahoma, v.1, p.53-129.

Reesor, J.E.
1958: Dewar Creek map-area with special emphasis on the White Creek Batholith, British Columbia; Geological Survey of Canada, Memoir 292, 78p.

1973: Geology of the Lardeau map-area, east-half, British Columbia; Geological Survey of Canada, Memoir 369, 129p.

1996: Geology of Kootenay Lake, British Columbia; Geological Survey of Canada, Map 1864A, scale 1:100 000.

Shives, R.B.K., Ford, K.L., and Charbonneau, B.W.

1995: Applications of gamma ray spectrometric/magnetic/VLF-EM surveys, Geological Survey of Canada, Open File 3061, 85p.

Slack, J.F., Shaw, D.R., Leitch, C.H.B., and Turner, R.J.W.

2000: Tourmalinites and Coticules from the Sullivan Pb-Zn-Ag Deposit and Vicinity, British Columbia: Geology, Geochemistry and Genesis; in The Geological Environment of the Sullivan Deposit, British Columbia, (ed.) J.W. Lydon, J.F. Slack, T. Höy, and M.E. Knapp; Geological Association of Canada, Mineral Deposits Division, MDD Special Volume No. 1, p.

Stinson, P. and Brown, D.A.

1995: Iron Range deposits, southeastern British Columbia (82F/1); in Geological Fieldwork 1994, (ed.) B. Grant B. and J.M. Newell; British Columbia Ministry of Energy, Mines and Petroleum Resources, Paper 1995-1, p.127-134.

Telford, W.M., Geldart, L.P., and Sheriff, R.E.

1990: Applied Geophysics, second Edition; Cambridge University Press, New York, 770p.

Turner, R.J.W., Leitch, C.H.B., Höy, T., Ransom, P.W., Hagen, A., and Delaney, G.D.

2000a: Sullivan Graben System: District-Scale Setting of the Sullivan Deposit; in The Geological Environment of the Sullivan Deposit, British Columbia, (ed.) J.W. Lydon, J.F. Slack, T. Höy, and M.E. Knapp; Geological Association of Canada, Mineral Deposits Division, MDD Special Volume No. 1, p.

Turner, R.J.W., Leitch, C.H.B., Ross, K.V., and Höy, T.;

2000b: District-scale Alteration Associated with the Sullivan Deposit, British Columbia, Canada; in The Geological Environment of the Sullivan Deposit, British Columbia, (ed.) J.W. Lydon, J.F. Slack, T. Höy, and M.E. Knapp; Geological Association of Canada, Mineral Deposits Division, MDD Special Volume No. 1, p.

Webber, G.L.

1979: Diamond drilling report on Vulcan group of mineral claims; British Columbia Ministry of Energy, Mines and Petroleum Resources, Assessment Report 7, 689p.

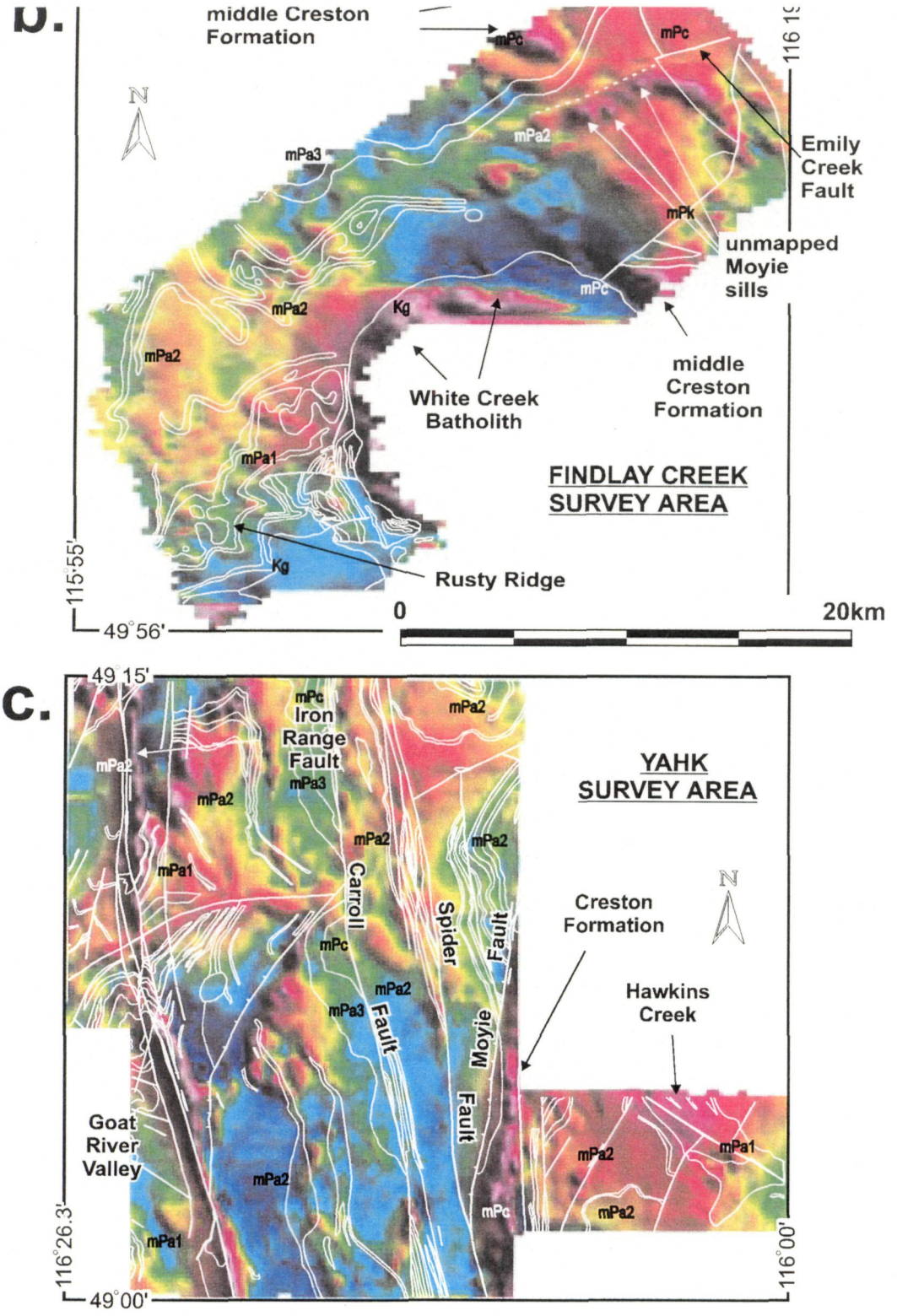

Figure C20-4. Magnetic anomaly data: **a**) St. Mary; **b)** Findlay; **c)** Yahk survey areas. High anomaly values are shown in hot colours and low anomaly values in cool colours. Geological boundaries from British Columbia Geological Survey Branch Geoscience Map 1995-1. Outcrops of Moyie sills are shown by fine dotted lines. Geological codes are as shown in Figure20-1b.

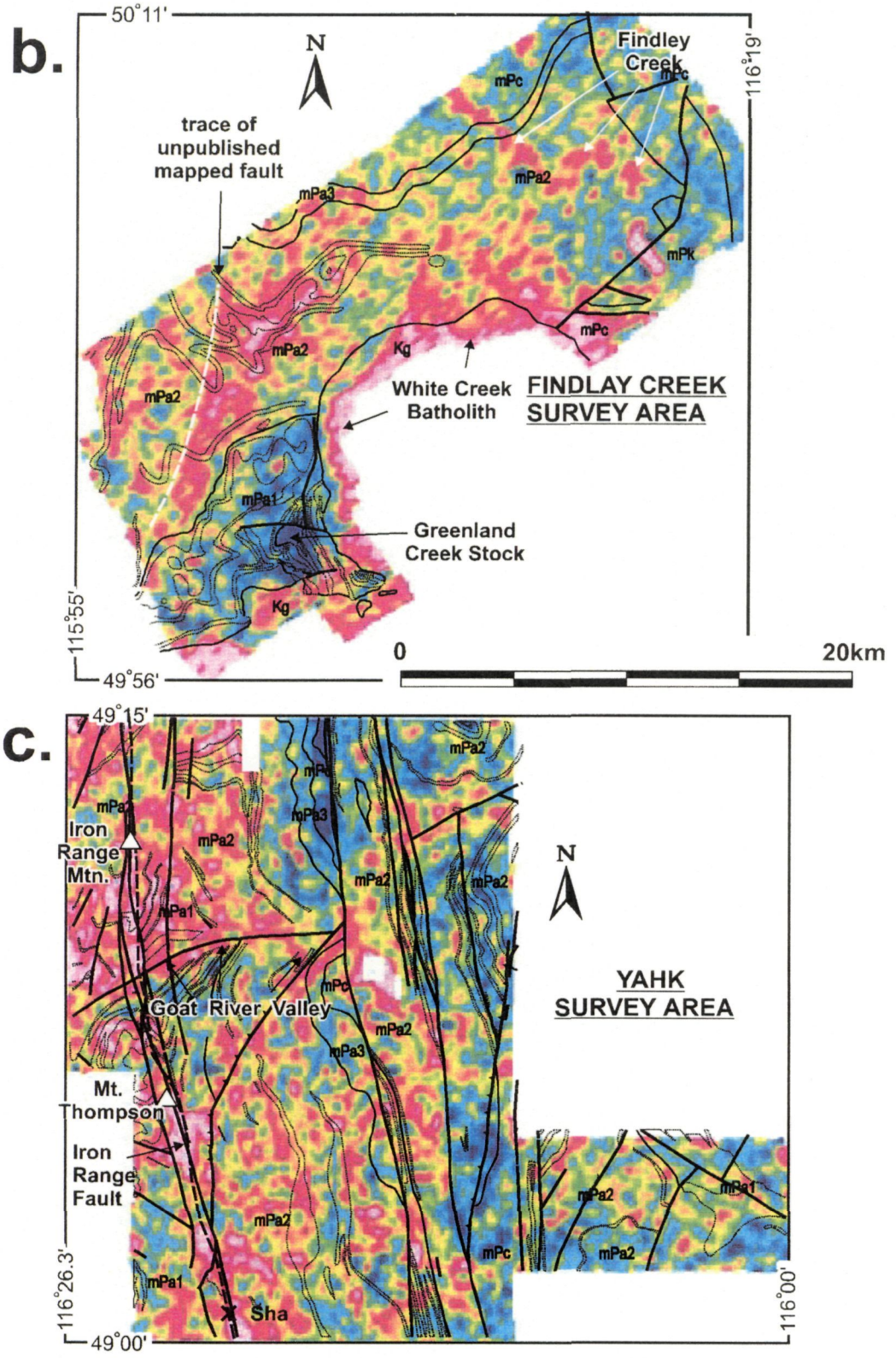

Figure C20-5. eTh/K levels: **a)** St. Mary; **b)** Findlay; **c)** Yahk survey areas. High values are shown in hot colours and low values in cool colours. Geological boundaries from British Columbia Geological Survey Branch Geoscience Map 1995-1. Outcrops of Moyie sills are shown by fine dotted lines. Geological codes are as shown in Figure20-1b.